

# 新型低功率與高雜訊抑制電生理訊號量測系統之前端 電路設計與分析

學生:林韋霆

指導教授:吳重雨 教授

電子工程學系電子研究所 碩士班

## 中文摘要



在無線網路的蓬勃發展下，許多結合無線網路的應用也由此應運而生。居家醫療看戶及遠距醫療即為其中的一項應用，而建構『電生理訊號量測與監控系統之無線化與晶片化』即為實現居家看護與遠距醫療的第一步。當一個生醫量測系統能夠結合無線網路時，我們便能夠在任何地方和任何時間下，輕易的監控一個人的身體狀況。

本論文將設計一個應用於『電生理訊號量測與監控系統』晶片之前端電路，在此前端電路中，包括了兩個部份：一個用以抑制人體雜訊之儀表放大器以及一個低頻的帶通濾波器。在本論文中，提出一個擁有高共模抑制比的儀表放大器，將有效抑制人體中大量的低頻雜訊，而後端的低頻帶通濾波器的設計將使用『跳蛙架構』(Leapfrog Structure)來減低元件飄移對於電路表現的影響。

此電生理訊號量測之前端電路，使用台灣積體電路 0.35 微米製程模擬，此電路第一級的儀表放大電路操作於 3.3 伏特，功率消耗為 0.1 毫瓦，頻寬為 2 至 16 千赫茲，有 0 至 60dB 之電壓增益，共模拒絕比率可達到 200 分貝至 250 分貝以抑制人體中之大量低頻雜訊。在此儀表放大器的後端，是一個可濾出不同所需人體

訊號之低頻濾波器，而此操作於 3.3 伏特下之低頻濾波器，功率消耗為 0.13 毫瓦，濾波器頻寬為 50 赫茲至 2 千赫茲，並有可調整之介於 0~60 分貝的電壓增益。整體的前端電路消耗 0.23 毫瓦，有 200 至 250 分貝之共模拒絕比率，頻寬為 2 至 16 千赫茲。



**THE DESIGN AND ANALYSIS OF NEW LOW POWER  
HIGH CMRR CMOS FRONT-END CIRCUITS FOR  
ELECTROPHYSIOLOGICAL SIGNAL  
MEASUREMENT SYSTEM**

**Student: Wei-Ting Lin**

**Advisor: Prof. Chung-Yu Wu**

**Department of Electronics Engineering & Institute of Electronics  
National Chiao Tung University**



**ABSTRACT**

With the growing development of wireless networks, many applications combined with wireless networks come into existence. Home nursing and remote medical care is one of the applications. And constructing the electrophysiological signals measurement and control system is the first step to realize the home nursing and remote medical care. While the measurement system is combined with wireless network, we can easily monitor the physical condition of people.

In this thesis, we will design the front-end circuit of the electrophysiological signals measurement and control system. The front-end circuit is composed of two parts, the instrumentation amplifier(INA) to compress the noise of human bodies and the low-frequency bandpass filter. In this thesis, we will announce a instrumentation amplifier with high common-mode rejection ratio (CMRR) which can effectively compress the noises in human bodies. The low-frequency bandpass filter behind the instrumentation amplifier uses leapfrog structure to decrease the influence on circuit performance due to devices variation.

The front-end circuits of the electrophysiological signals measurement simulates with TSMC 0.35um technology. The first stage INA operates at 3.3V, consumes the power of 0.1mW. Its bandwidth is between 2~16 kHz, and its CMRR archives the magnitude 200~250 dB to suppress the enormous low-frequency noises in human bodies. Behind the INA is the low-frequency bandpass filter which filters different human-body signals. The low-frequency bandpass filter operates at 3.3V and consumes 0.13mW. Its bandwidth is from 50Hz to 2kHz and has the tunable gain between 0~60dB.



# ACKNOWLEDGEMENTS

首先我要感謝我的指導老師吳重雨教授多年來耐心的指導與鼓勵，使我能夠順利完成碩士學位。在吳教授循序漸進的諄諄教誨下，除了讓我獲得許多積體電路設計的專業知識外，更學習到挑戰困難及解決問題的態度與方法，而在與國外的學術交流中，也讓我因此拓展了國際的視野。這些的訓練與磨練也讓我在交大電子所的這幾年來，成長許多。

此外，在這段求學過程中，感謝 307 實驗室豐富的軟硬體資源以及幫忙建立這些資源的人員們，由於你們辛苦的維護與建立這些軟硬體資源，讓我能夠在這樣的環境中，順利的利用這些資源來完成我的研究以及碩士論文。

其次我要感謝施育全、鄭秋宏、廖以義、黃冠勳、林俐如、王文傑、江政達、蘇烜毅、虞繼堯、黃鈞正等學長姐們，對我在研究上面的指導以及幫助。另外還要感謝陳勝豪、陳旻玟、陳煒明、黃祖德、蔡夙勇、楊文嘉、顏承正、蕭淵文、盧台祐、陳建文、吳書豪、曾瑋信、李宗霖、丁彥、謝致遠、黃如琳、蕭勝文、莊凱嵐、郭秉捷、林棋樺等實驗室同學們，一起研究課業以及在生活上的相互幫助，陪伴我度過這些年來的研究生涯，希望大家都能在學業或工作上順順利利。

另外，我要感謝我的朋友，丕哥、毓康、思瑋、俊憬、雲清、銘德、一斌、牛、智堯、志偉、小山、清大口琴社的夥伴以及附中 875 的好同學們，謝謝你們，有你們陪伴的出遊、打球、以及生活上的分享及幫助，讓我在研究之餘，也能夠有一個非常快樂開心的休閒生活。

最後，我要感謝我親愛的父親林炳輝，母親廖伶玉，弟弟林哲雋以及一直耐心陪伴著我的資穎，謝謝你們對我無怨無悔的支持，我才能一路這樣的走過來，你們一向是我努力的原動力，我愛你們，尤其是媽媽的細心栽培與無悔的付出，才会有今天的我。把這份論文獻給我最愛的你們。

林韋霆  
誌於 風城交大  
九五年七月

# Contents

<b>Chinese Abstract .....</b>	<b>i</b>
<b>English Abstract .....</b>	<b>iii</b>
<b>Contents.....</b>	<b>vi</b>
<b>Table Captions.....</b>	<b>viii</b>
<b>Figure Captions .....</b>	<b>ix</b>
<b>Chapter 1 INTRODUCTION.....</b>	<b>1</b>
<b>1.1 BACKGROUND .....</b>	<b>1</b>
<b>1.2 REVIEW ON ELECTROPHYSIOLOGICAL SIGNAL MEASUREMENT SYSTEM.....</b>	<b>4</b>
<b>1.2.1 Review of Instrumentation Amplifier Structures.....</b>	<b>4</b>
<b>1.2.2 Review of Low-Frequency Bandpass Filter Structures .....</b>	<b>11</b>
<b>1.3 MOTIVATIONS .....</b>	<b>16</b>
<b>1.4 THESIS ORGANIZATION .....</b>	<b>17</b>
<b>Chapter 2 ARCHITECTURE AND CIRCUITS DESIGN .....</b>	<b>19</b>
<b>2.1 ARCHITECTURE DESIGN OF THE INSTRUMENTATION AMPLIFIERS .....</b>	<b>19</b>
<b>2.1.1 Differential difference operational amplifier (DDA).....</b>	<b>19</b>
<b>2.1.2 Differential difference operational transconductance amplifier (DDGM).....</b>	<b>20</b>
<b>2.1.3 New structure design of the instrumentation amplifier .....</b>	<b>20</b>
<b>2.2 CIRCUIT DESIGN OF THE DIFFERENTIAL DIFFERENCE OPERATIONAL .....</b>	
<b>TRANSCONDUCTANCE AMPLIFIER .....</b>	<b>24</b>
<b>2.2.1 The Flipped Voltage Follower (FVF).....</b>	<b>24</b>
<b>2.2.2 The differential difference operational transconductance amplifier.....</b>	<b>26</b>
<b>2.3 ARCHITECTURE DESIGN OF THE LOW-FREQUENCY BANDPASS FILTER .....</b>	<b>27</b>
<b>2.3.1 Specification of the low-frequency bandpass filter.....</b>	<b>27</b>

2.3.2 LC network and the leapfrog structure.....	28
2.3.3 Gm-C filter .....	32
<b>2.4 CORE CIRCUIT DESIGN OF THE FILTER.....</b>	<b>36</b>
2.4.1 The Gm amplifier using the mos resistor .....	36
2.4.2 The nonideal effects of the Gm amplifiers .....	38
<b>Chapter 3 SIMULATION RESULTS .....</b>	<b>44</b>
3.1 SIMULATION RESULTS OF THE FLIPPED VOLTAGE FOLLOWER (FVF) .....	44
3.2 SIMULATION RESULTS OF THE GM AMPLIFIER .....	45
3.3 SIMULATION RESULTS OF THE INSTRUMENTATION AMPLIFIERS .....	46
3.4 SIMULATION RESULTS OF THE LOW-FREQUENCY BANDPASS FILTER .....	50
3.5 WHOLE SIMULATION OF THE FRONT-END ELECTROPHYSIOLOGICAL SIGNAL MEASUREMENT SYSTEM.....	53
<b>Chapter 4 CONCLUSIONS AND FUTURE WORKS</b>	
4.1 CONCLUSIONS.....	55
4.2 FUTURE WORKS .....	56

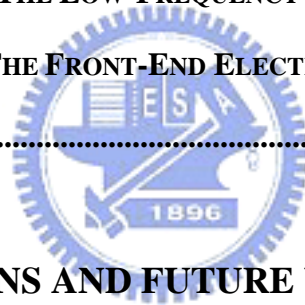


## Table Captions

Table 2.1 The size of the DDGm amplifier in Fig. 2.10.....	27
Table 2.2 The specification of the low-frequency bandpass filter .....	28
Table 2.3 Gm values of the Gm amplifier in Fig. 2.17 .....	35
Table 2.4 The size of the DDGm amplifier in Fig. 2.10.....	37
Table 3.1 Simulation results of the INA.....	50
Table 3.2 Simulation results of the low-frequency BP filter.....	52
Table 3.3 Simulation results of the front-end circuit of the electrophysiological signal measurement system.....	54





# Figure Captions

## CHAPTER 1

Fig. 1.1 Schematic block diagram of the biotelemetry system.....	3
Fig. 1.2 Conventional Three-op instrumentation amplifier.....	5
Fig. 1.3 The symbol and the matrix form of second generation current conveyor .....	5
Fig 1.4 Conventional current-mode instrumentation amplifier.....	6
Fig. 1.5 Current-mode instrumentation amplifier using current cancellation by an operational amplifier .....	7
Fig. 1.6 Current-mode instrumentation amplifier using current inversion.....	8
Fig. 1.7 Current-mode instrumentation amplifier.....	9
Fig. 1.8 Current-mode instrumentation amplifier using bias current sensing of opamps .. .....	10
Fig. 1.9 Choice of filter type as a function of the operating frequency range .....	12
Fig. 1.10 The Nauta's Gm amplifier .....	13
Fig. 1.11 The rail-to-rail Gm amplifier .....	14
Fig. 1.12 The conventional Gm amplifier .....	15
Fig. 1.13 Common-drain amplifier (voltage follower).....	16
Fig. 1.14 Common-drain amplifier with output loads.....	16

## CHAPTER 2

Fig. 2.1 The symbol for Differential Difference Operational Amplifier.....	19
Fig. 2.2 The symbol for Differential Difference Operational Transconductance Amplifier .....	20
Fig 2.3 Expression for the new approach of instrumentation amplifier .....	21
Fig 2.4 Subtraction of input signals using two DDGm .....	22

Fig. 2.5 The new structure of high CMRR instrumentation amplifier .....	23
Fig. 2.6 The function of the first stage and waveform of $V_{x1}$ and $V_{x2}$ .....	23
Fig. 2.7 Flipped Voltage Follower (FVF) .....	25
Fig. 2.8 The DDGm amplifier using FVF method .....	26
Fig. 2.9 (a) The prototype LC network of the 5th-order Elliptic bandpass filter	
(b) The LC network after element value normalization.	
(c) The LC network after element position change for leapfrog structure .....	29
Fig. 2.10 (a) The LC network of the 5th-order BP Elliptic filter	
(b) The block diagram of leapfrog structure for the 5th-order BP Elliptic filter	
(c) The block diagram of leapfrog structure for the 5th-order BP Elliptic filter	
.....	30
Fig. 2.11 The simulation result of 5 <sup>th</sup> -order Elliptic LC ladder .....	31
Fig. 2.12 Circuits implementations for functions of the functions in Fig 2.10 .....	32
Fig. 2.13 The two port network of Gyrator .....	33
Fig. 2.14 (a) The realization of a grounded inductor	
(b) The realization of a floating inductor.....	33
Fig. 2.15 (a) The realization of a grounded inductor composed of Gm and capacitor	
(b) The realization of a floating inductor composed of Gm and capacitor....	34
Fig. 2.16 The low-frequency bandpass Gm-C filter with leapfrog structure .....	35
Fig. 2.17 The circuit of the Gm amplifier .....	36
Fig. 2.18 The circuit of the Gm amplifier connected with MOS resistor.....	37
Fig. 2.19 The method to eliminate the background current of the Gm amplifier.....	39
Fig. 2.20 The finite Ro of Gm amplifier in the Gyrator .....	40
Fig. 2.21 The Gm amplifier with a capacitor load .....	41
Fig. 2.22 The transfer function of the filter with ideal and nonideal Gm.....	42

Fig. 2.23 The output stage of the Gm amplifier .....	43
--	----

### CHAPTER 3

Fig. 3.1 The gain comparison of the conventional voltage follower and FVF versus $R_G$ .....	44
Fig. 3.2 The frequency response of the Gm amplifier with different Gm values.....	45
Fig. 3.3 The frequency response of the Gm amplifier with nA/V Gm values .....	45
Fig. 3.4 The calculated and HSPICE simulated Iout versus $R_G$ .....	46
Fig. 3.5 The differential-mode signal of node $V_{x1}$ and $V_{x2}$ .....	47
Fig. 3.6 The common-mode signal of node $V_{x1}$ and $V_{x2}$ .....	47
Fig. 3.7 The frequency response of the proposed INA structure.....	48
Fig. 3.8 The frequency response of the proposed INA structure with four corners .....	48
Fig. 3.9 The HSPICE Monte-Carlo simulation of the frequency response of the proposed INA structure .....	49
Fig. 3.10 Simulation results with the comparison of the ideal and the realistic filter ...	51
Fig. 3.11 Simulation results of the low-frequency BP filter with four corners .....	52
Fig. 3.12 The differential and common mode simulation results front-end circuit of the electrophysiological measurement system .....	53

# CHAPTER 1

## INTRODUCTION

---

### 1.1 BACKGROUND

With the increase of ageing population, chronic diseases, and need for further integration of handicapped through rehabilitation, monitoring, homecare, the development of healthcare and health delivery is constantly progressing.

As the combination of medical care and integrated circuits, the biotelemetry system for monitoring and measuring electrophysiological signals are paid more and more attention nowadays. When a biomedical system is integrated with radio transceivers, we can easily monitor the patient's physical condition everywhere. So that home nursing and remote medical care will be realized [1]-[2].

In the biomedical measurement system, the measurement and wireless transformation of electrophysiological signals can be realized for a single chip by SoC technology. This technique makes people who need nursing can wear the biomedical measurement system. Therefore we can monitor the electrophysiological signals and transfer the signals to the Remote host anywhere at any time.

During the last few years the research and development on smart wearable for remote health monitoring have been accelerated through consequent public and private financial support. Remote health monitoring could lead to a significant reduction of total cost in healthcare by avoiding unnecessary hospitalizations and ensuring that those who need urgent care get it sooner. To meet the requirements of smart wearable worn

by the subject, it is necessary to develop the miniaturized, low power, and wireless biomedical sensors.

Portable biomedical sensors of detecting EMG (Electrocardiography), EEG (Electroencephalography), and ECG (Electromyography) signals have been developed and commercialized. However, for implementing the remote health monitoring under the normal quality of life, these biomedical sensors must be wireless link between the subject and the majority of the signal processing system, and be miniaturized via System-on-Chip (SoC) technology.

A biotelemetry system consisting of portable and stationary parts has been developed to monitor and analyze the biomedical signals ECG and EMG [3]. This system was not miniaturized by using SoC technology yet. A particularly strong emerging trend is the move toward SoCs that can provide low-data-rate, short-range wireless communications. Moreover, highly integrated, mixed-signal SoC solutions are ideal for medical OEMs looking to increase the functionality of implantable and portable medical applications.

Because the biomedical measurement system is realized for chip, we can easily combine it with our mobile system, like PDA, notebook, PC, and mobile phones. Through proper software we can make these consuming IT products become valuable homecare and remote medical apparatus.

Consequently, many researches on the biomedical systems are proposed. Fig.1.1 shows the block diagram of the whole biotelemetry system. In the biotelemetry system, RF signals from the portable subsystem will be transmitted to the stationary system which monitors people's physical conditions.

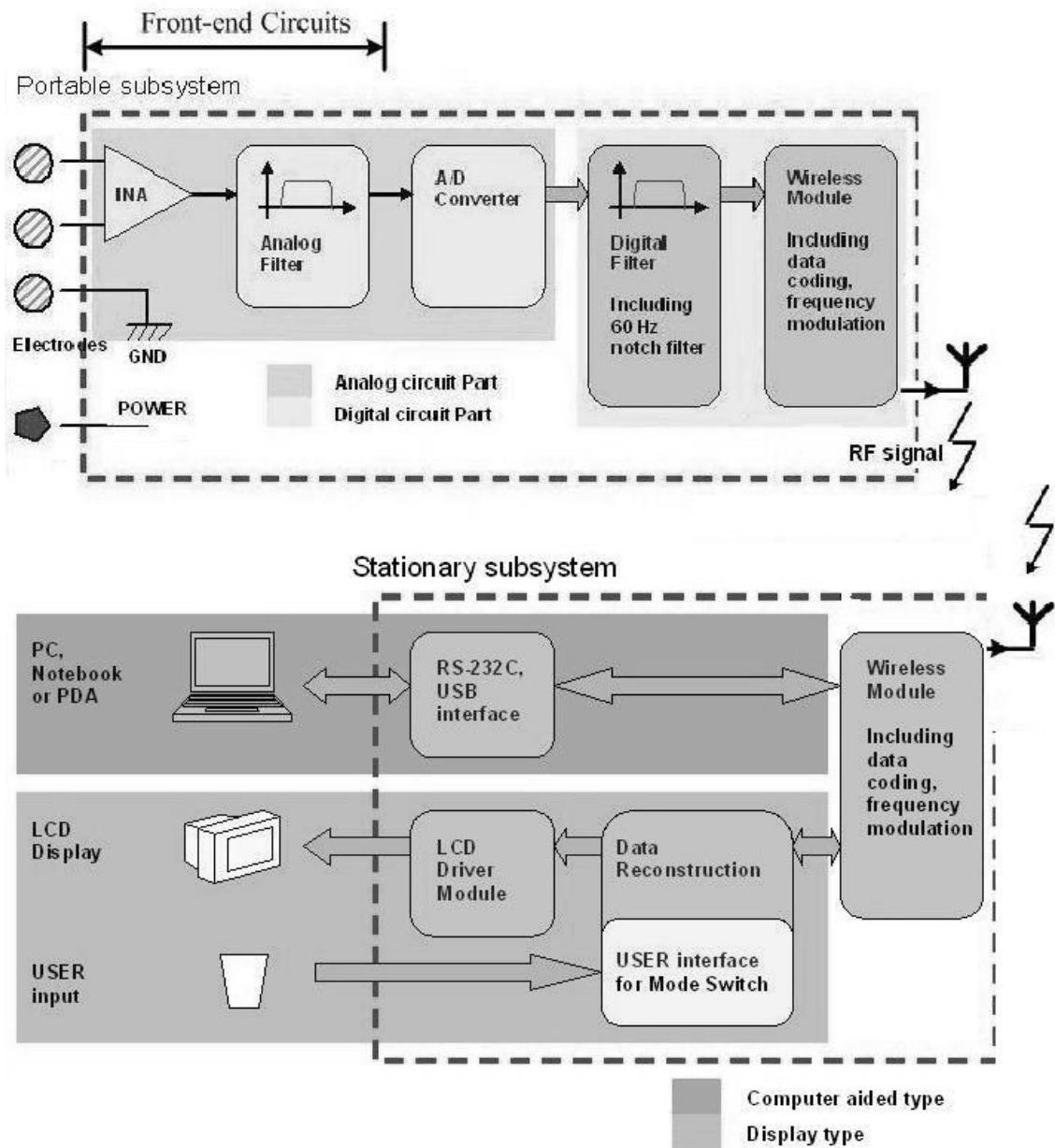


Fig. 1.1 Schematic block diagram of the biotelemetry system

## 1.2 REVIEW ON ELECTROPHYSIOLOGICAL SIGNAL MEASUREMENT SYSTEM

### 1.2.1 Review on Instrumentation Amplifier Structures

#### (1) Voltage-mode Instrumentation amplifiers

The most often used instrumentation amplifier is constructed of three operational amplifiers and seven resistors showed in Fig. 2.1. The first stage with two opamp op1 & op2 and  $R_1$  &  $R_2$  &  $R_G$  is responsible for amplifies input signals  $V_{in+}$  &  $V_{in-}$ . And the voltage gain is

$$A_d = \left(1 + \frac{2R_1}{R_G}\right) \quad (1.1)$$

So we can adjust  $R_G$  which is tunable to obtain the gain we want. The function of the second stage with op3 and  $R_3 \sim R_6$  is to counteracts common-mode signals and add differential signals. So we can obtain good common-mode rejection ratio (CMRR) and take away the noises we don't want.

But there exists a disadvantage in this kind of structure. In Fig2.1, we can find the output signal  $V_{out}$  is

$$V_{out} = V_+ \times \left(-\frac{R_4}{R_3}\right) + V_- \times \left(\frac{R_6}{R_5 + R_6} \cdot \frac{R_3 + R_4}{R_3}\right) \quad (1.2)$$

As a result, we need a very good resistors matching of  $R_3 \sim R_6$  to make  $\frac{R_4}{R_3} = \frac{R_6}{R_5}$  if we want  $V_{out}$  almost equals to zero when  $V_+ = V_- \approx V_{CM} \cdot A_d$  -- otherwise the CMRR will degrade seriously.

Another problem in this kind of structure is that when we have gain error or the gain is not high enough in op1 and op2, we will have output voltage error. Ref [4] provides a good method to lower the output voltage error of this kind of structure.

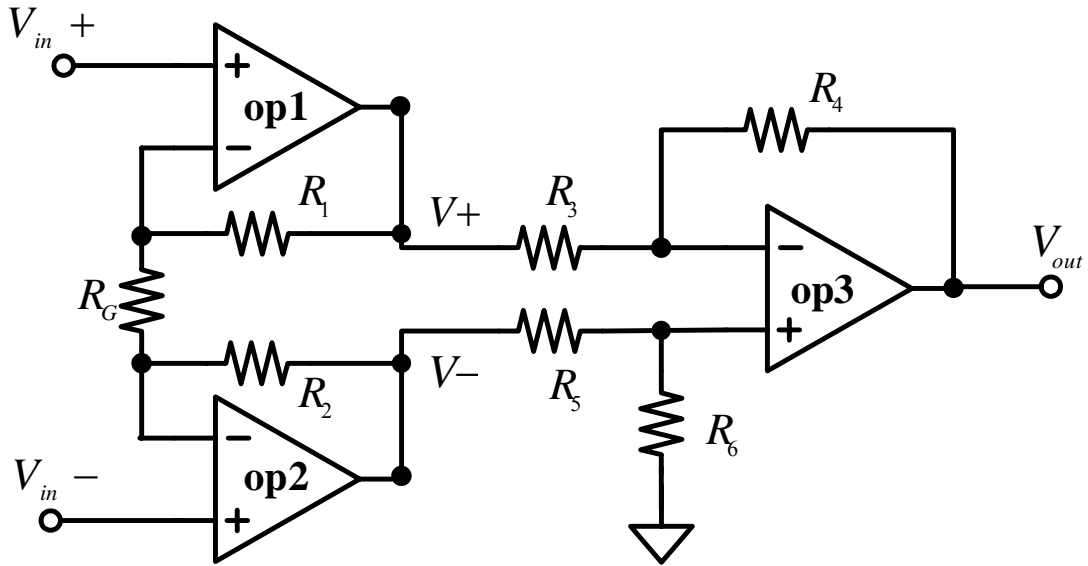
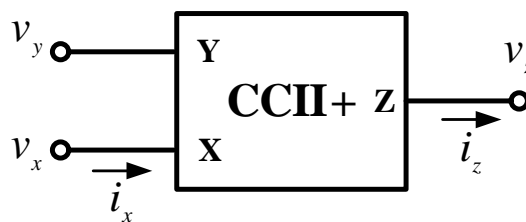


Fig. 1.2 Conventional Three-op instrumentation amplifier

## (2) Current-mode Instrumentation amplifiers

Because of the disadvantage of the conventional voltage-mode instrumentation amplifier, many researches on current-mode instrumentation amplifier comes into existence. In most of the current-mode instrumentation amplifiers, the second generation current conveyor is an important block and the idea of current subtraction is also widely used [5]. We'll introduce these concepts in the following sections.



$$\begin{bmatrix} i_y \\ v_x \\ i_z \end{bmatrix} = \begin{bmatrix} 0 & 0 & 0 \\ 1 & 0 & 0 \\ 0 & \pm 1 & 0 \end{bmatrix} \cdot \begin{bmatrix} v_y \\ i_x \\ v_z \end{bmatrix}$$

Fig. 1.3 The symbol and the matrix form of second generation current conveyor



### (a) Conventional Current-mode Instrumentation amplifiers

Current conveyor is widely used in many current-mode circuits [6]. The conventional current-mode instrumentation amplifier is also constructed of the second generation current conveyor (CCII). The conventional current-mode instrumentation amplifier is showed in Fig. 1.4. It has the voltage gain  $R_2 / R_1$ , and it doesn't need a good resistor matching to reach high CMRR. The amplifier's bandwidth is large with high voltage gain as current conveyors are operating in open loop without the gain-bandwidth product limitation.

Unlike the voltage-mode instrumentation amplifier mentioned before, the CMRR of the current –mode instrumentation amplifier is independent of the voltage gain. And due to these characters, the current –mode instrumentation amplifier is good for low-gain and wide-bandwidth applications.

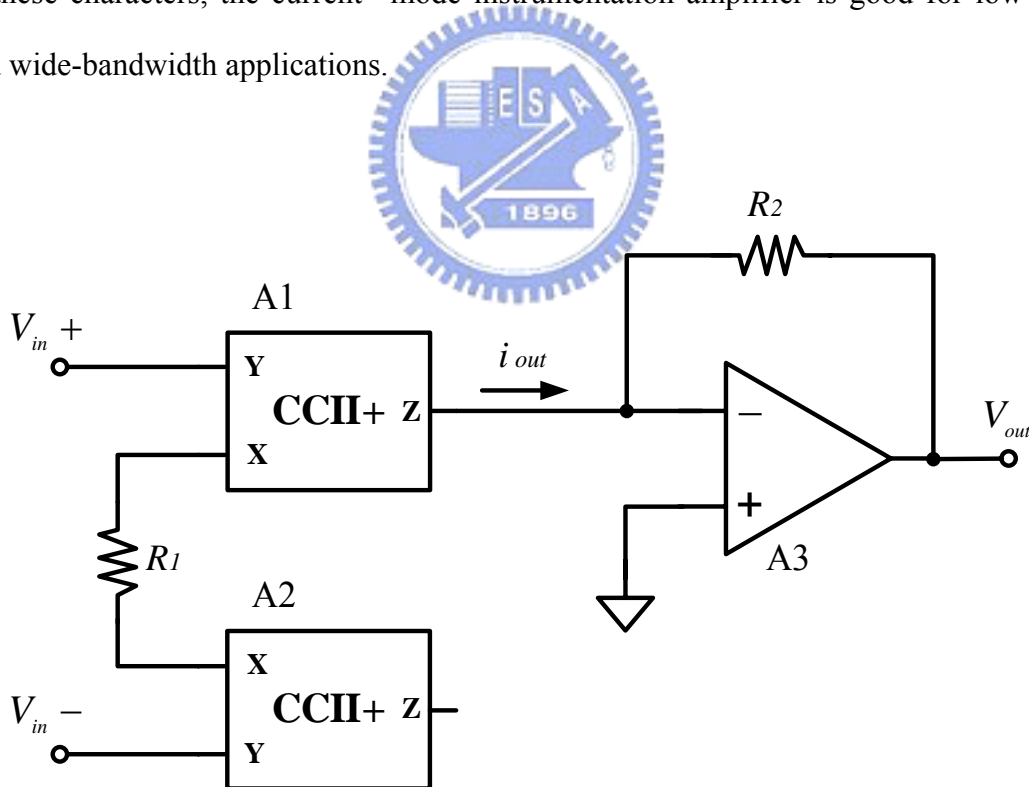


Fig. 1.4 Conventional current-mode instrumentation amplifier

## (b) Current-mode Instrumentation amplifier using CCII with current cancellation

Although the conventional current-mode instrumentation amplifier doesn't need good resistor matching, its CMRR is not high enough [6]. So we can use current subtraction to improve it. It can effectively improve CMRR of the current-mode instrumentation amplifier. Fig. 1.5 is the current-mode instrumentation amplifier using current cancellation by operational amplifier. Once there is common-mode current  $i_1$  flowing to output, it will use  $i_2$  to cancel the common-mode signal. And we can adjust the value of  $R_3$  to improve the CMRR. But the disadvantage of this structure is that the frequency range of CMRR will be restricted by the operational amplifier. So the frequency range would be limited, and it won't be such wideband as the structure mentioned before.

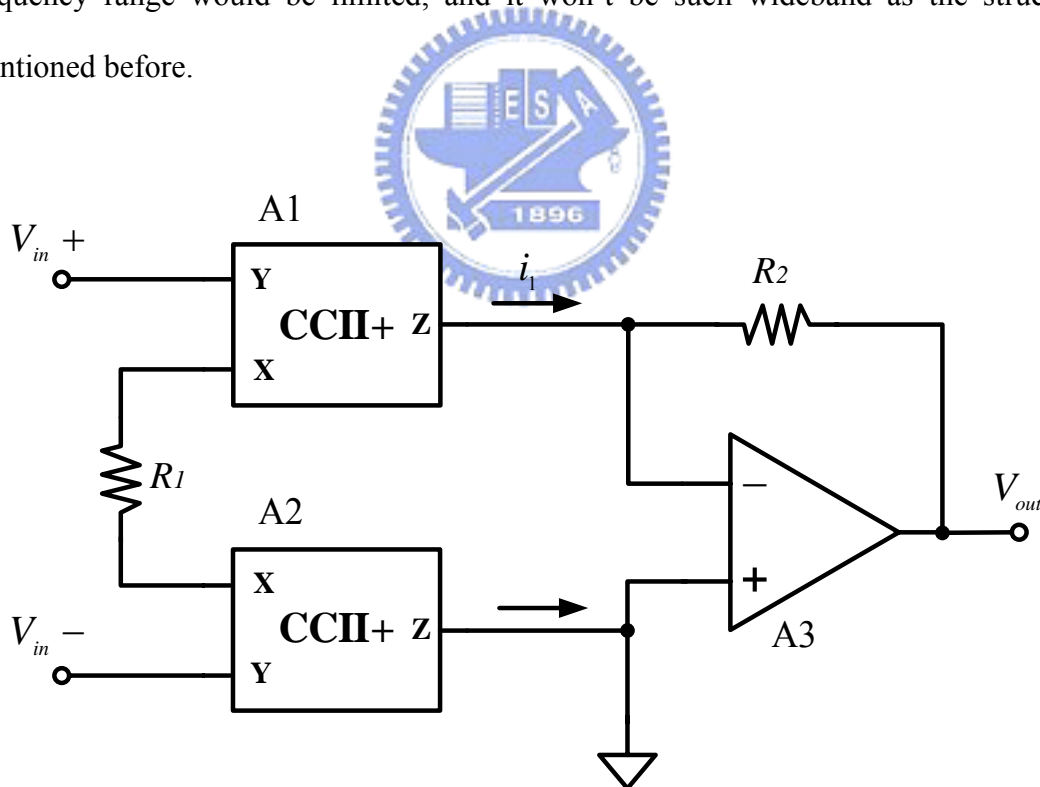


Fig. 1.5 Current-mode instrumentation amplifier using current cancellation by an operational amplifier

**(c) Current-mode Instrumentation amplifier using CCII for current inversion**

As mentioned in section (2), the structure of current cancellation by an operational amplifier can't achieve wide bandwidth. This problem can be solved by current inversion method [6]. Current inversion can be realized by inverting the second conveyor output current with an additional positive second-generation current conveyor CCII and summing it then up with the first conveyor output current as presented in Fig. 1.6. The RC network adding to the first current conveyor can make the summing range more accurate. Besides, this network can compensate for the high frequency phase shift of the added conveyor but the resistance  $R_3$  can also compensate for the systematic current transfer error, due to the finite input and output impedance of the conveyor. Comparing to the conventional current-mode instrumentation amplifier, this current inversion structure is also insensitive to the gain error of the CCII.

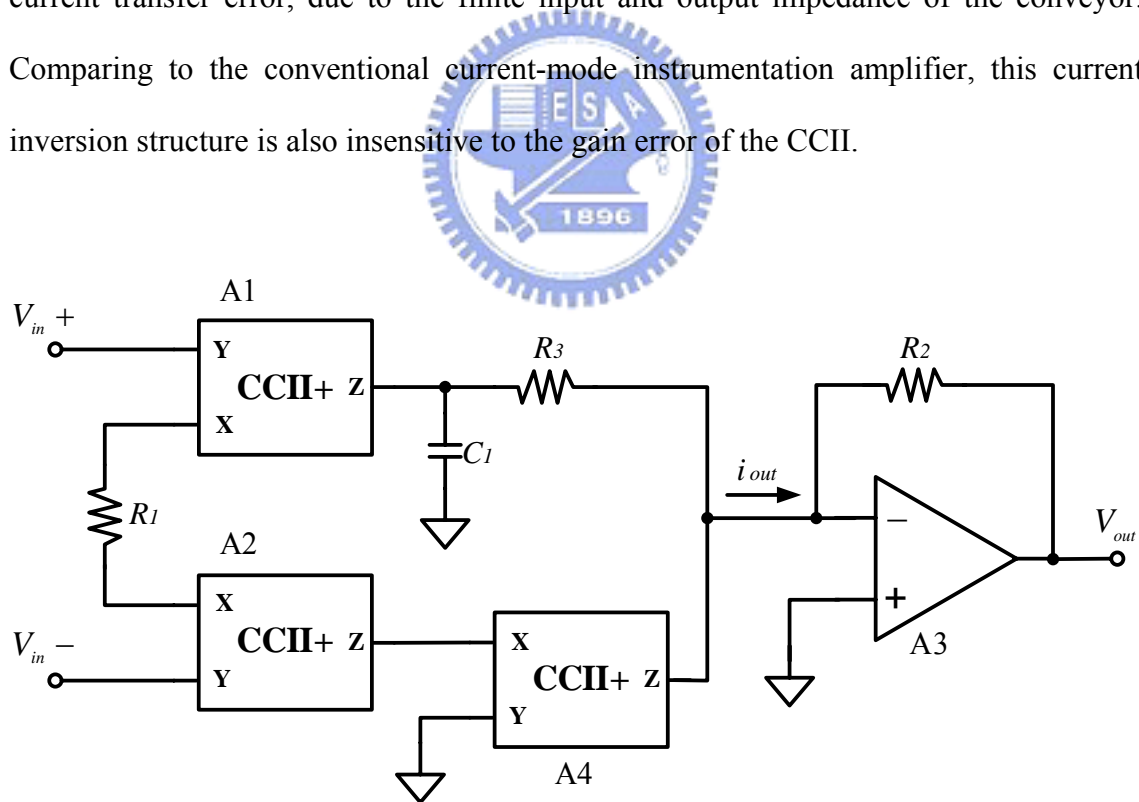


Fig. 1.6 Current-mode instrumentation amplifier using current inversion

Another structure published in [7] uses the similar concept to eliminate the current of common mode. The structure is showed in Fig. 1.7 and the node Z of A1 is

connected to the node X of A2. It forms a feedback and it minimizes the output current of A1. Therefore the common-mode gain would be compressed.

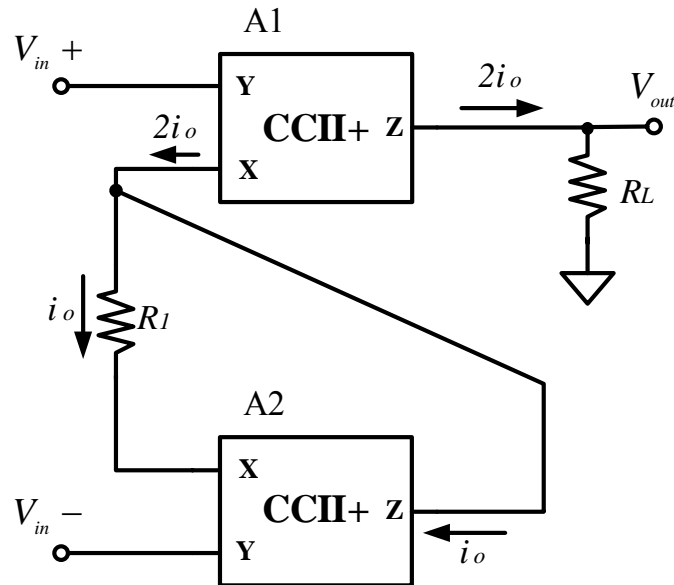


Fig. 1.7 Current-mode instrumentation amplifier

#### (d) Current-mode Instrumentation amplifier using bias current sensing of opamps

In measuring small biomedical signals, differential amplifiers are often applied to overcome the interference of noises in human bodies. Therefore current-mode instrumentation amplifiers using differential operational amplifiers are also presented in many papers. In Ref [8], the method of bias current sensing is presented and the schematic of this structure is presented in Fig. 1.8. The input stage consists of two identical opamps connected as unity-gain buffer. The outputs of the two opamps are connected via  $R_7$  like the conventional three-op INA. The input voltages transfer to current  $i_x$  through  $R_7$  and the current  $i_x$  flows through the bias circuit of op1. After  $I_{BIAS} + i_x$  and  $i_x$  flow through the two current mirrors and the subtraction of these two branches of current. The current  $i_x$  will flow through  $R_8$  and forms the output voltage  $V_{out}$ . The function of op3 is to prevent the value of  $R_8$  affecting the output impedance of the first stage of op1 & op2.

There are two main advantage of this structure compared to the three-op INA. The first is that no resistor matching is required to achieve high CMRR. The second advantage is that this structure doesn't require ideal opamps; the design requires only that the opamps identical. But the goal is difficult to attain, but it is easier than having an ideal opamp.

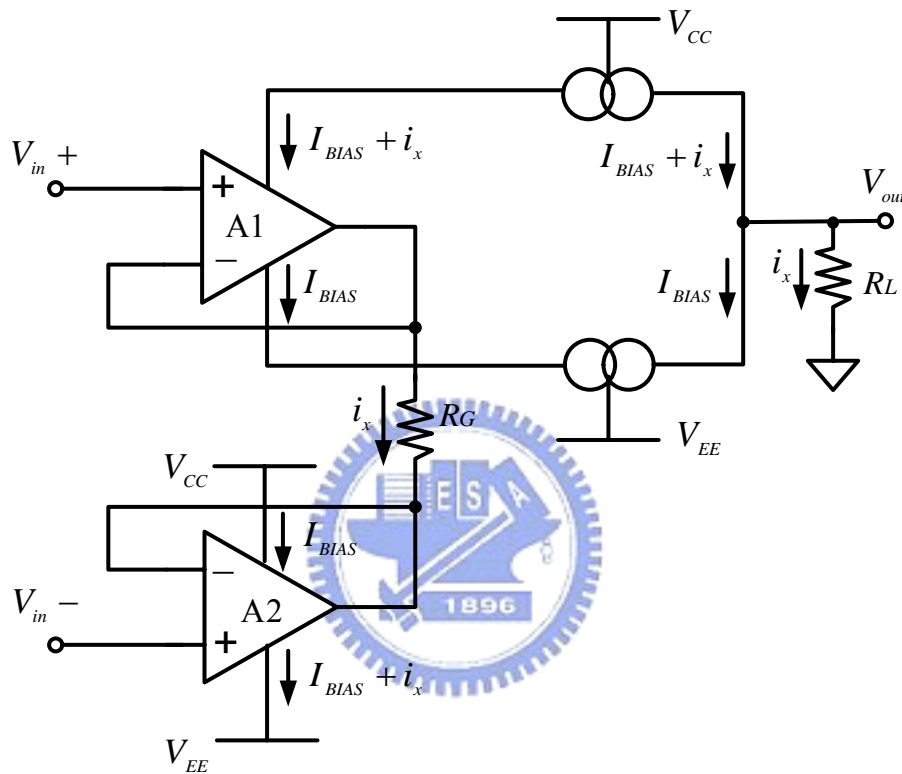


Fig. 1.8 Current-mode instrumentation amplifier using bias current sensing of opamps

But there is a serious disadvantage of this kind of structure that we need a precise current mirror to make the current  $I_{BIAS} + i_x$  and  $I_{BIAS}$  subtracted to  $i_x$  perfectly. Once the two current mirrors don't match well, we will not have a good CMRR. So the design of the current mirror is the main point of this structure to obtain good performance.

Another kind of current-mode instrumentation amplifier structure is also published in [9]. It uses the similar method of current-mode instrumentation amplifier using current inversion we introduced before.

## 1.2.2 Review on Bandpass Filter Structures

### (1) Comparison on Different Filter Types

From the derivations of mathematical sentences, we can get different transfer functions and responses. There are four essential filter types widely used in the design of filters: Butterworth, Chebyshev, Inverse Chebyshev and Elliptic filter. According to different requirements, we can choose the type we need. Here we'll introduce these four filter types.

	Filter Type
Order	Elliptic > Inv-Che > Chebyshev > Butterworth
Passband performance	Butterworth > Inv-Che > Chebyshev or Elliptic
Group delay	Elliptic > Butterworth > Inv-Che > Chebyshev

### (2) Design considerations

We have introduced the passive and active filters and analysis the advantages and disadvantages of them. We can choose the type we need from the characteristics from them and the following are the consider factors we must consider when designing a filter:

1. The technology desired for the system implementation.
2. Availability of dc supplies for the active devices, and power consumption.
3. Cost
4. The range of frequency of operation.
5. The sensitivity to parameter changes and stability.
6. Weight and size of the implemented circuit.
7. Noise and dynamic range of the realized filter.

Also, filtering requirements at very high frequencies where ultra fast sampling and digital circuitry may not be realistic and economical may require analog techniques. We'll show the choice of filter types as a function of the operating frequency range. Fig.

1.9 shows the adequacy frequency range of different type filters.

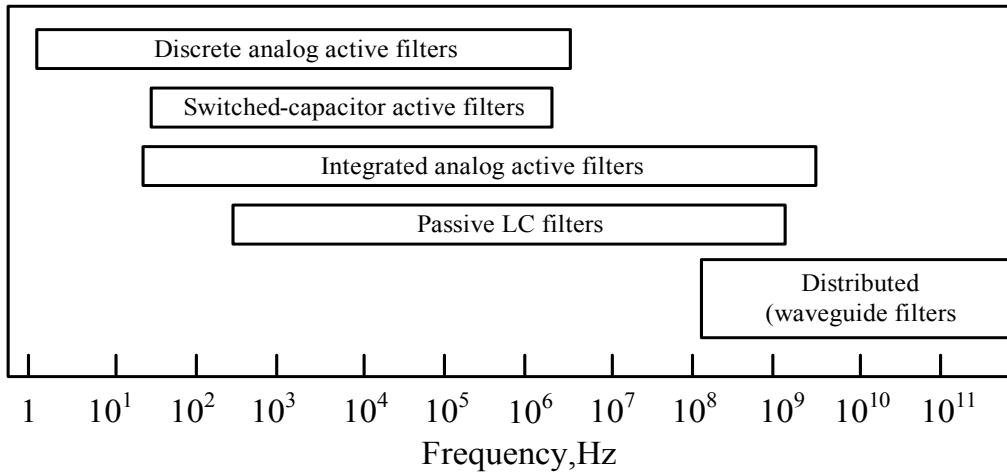


Fig. 1.9 Choice of filter type as a function of the operating frequency range

## 1.2.2 Review on Gm amplifiers

### (1) Different Gm amplifiers

Gm amplifier is a widely used and important analog block in analog circuits like filters and other current-mode circuit. The Gm amplifier transfers voltage to current and is also called the operational transconductance amplifier. The following is the review on some Gm amplifiers.

#### (a) Nauta's Gm amplifier

There is a Gm amplifier proposed in [10]-[11] by Nauta and shown in Fig. 1.10. From Fig. 1.10, we can find that the Gm amplifier has no internal nodes, so it can achieve high bandwidth and operate at high frequency filters or robust low frequency filters. The Gm value of the amplifier is shown as below:

$$G_m = (V_{dd} - V_m + V_{tp}) \sqrt{k_n' k_p' \left( \frac{W_n}{L_n} \right) \left( \frac{W_p}{L_p} \right)} \quad (1.3)$$

Although the Gm amplifier has wide bandwidth, it has some disadvantage that its Gm value is decided by MOS parameters and is easily changed by process variation. In Gm-C filters, we need precise Gm value to maintain the performance of the filter. Also the Gm value decided by MOS parameters is fixed and cannot be tuned after been

manufactured. From (1.3), we can find that if we need large  $G_m$  value, we need either large size MOS or to consume more power.

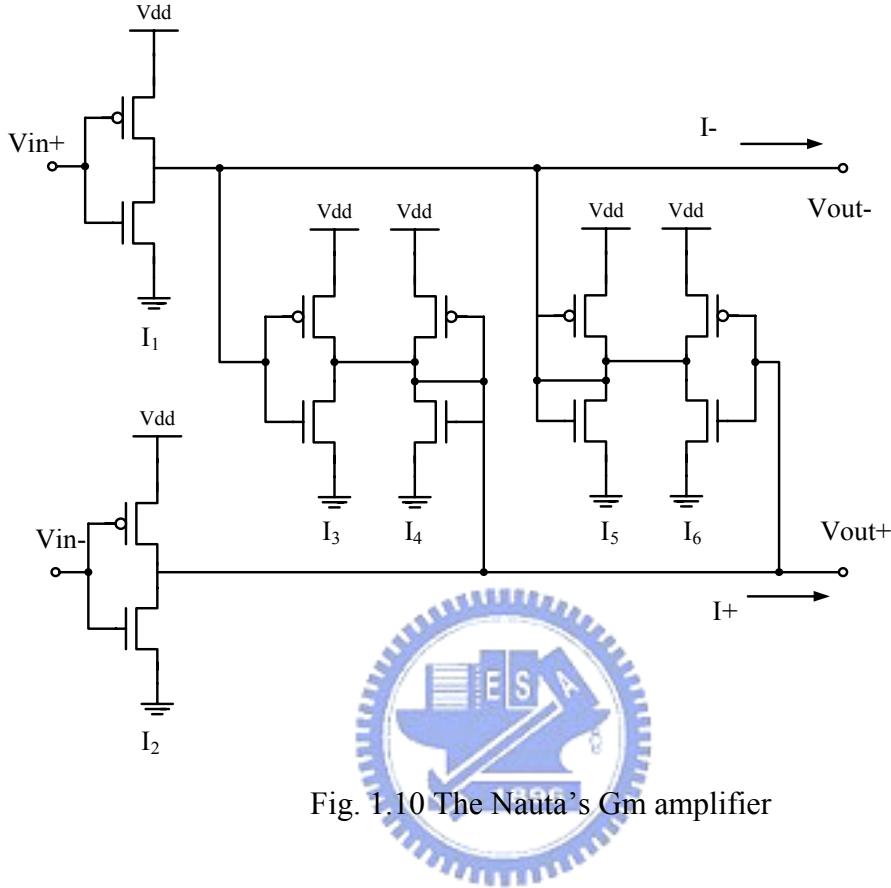


Fig. 1.10 The Nauta's  $G_m$  amplifier

### (b) Rail-to-rail $G_m$ amplifier

Another  $G_m$  amplifier proposed in [12] is a rail-to-rail  $G_m$  amplifier shown in Fig. 1.11. It can operate with full input swing and used in high input signal applications. Its  $G_m$  value is shown as below:

$$G_m = \frac{K_n' K_{na}' (V_{cm} - V_m)(V_1 + V_2 - 2V_m)}{K_p'} \quad (1.4)$$

This rail-to-rail  $G_m$  amplifier can have multiple outputs by put parallel output stages as M6 and M6a. However, it has the same problem like Nauta's  $G_m$  amplifier that its  $G_m$  value is fixed and will be affected by process variation. Besides, it also consumes large power or occupies large size MOS when large  $G_m$  value is going to be realized.



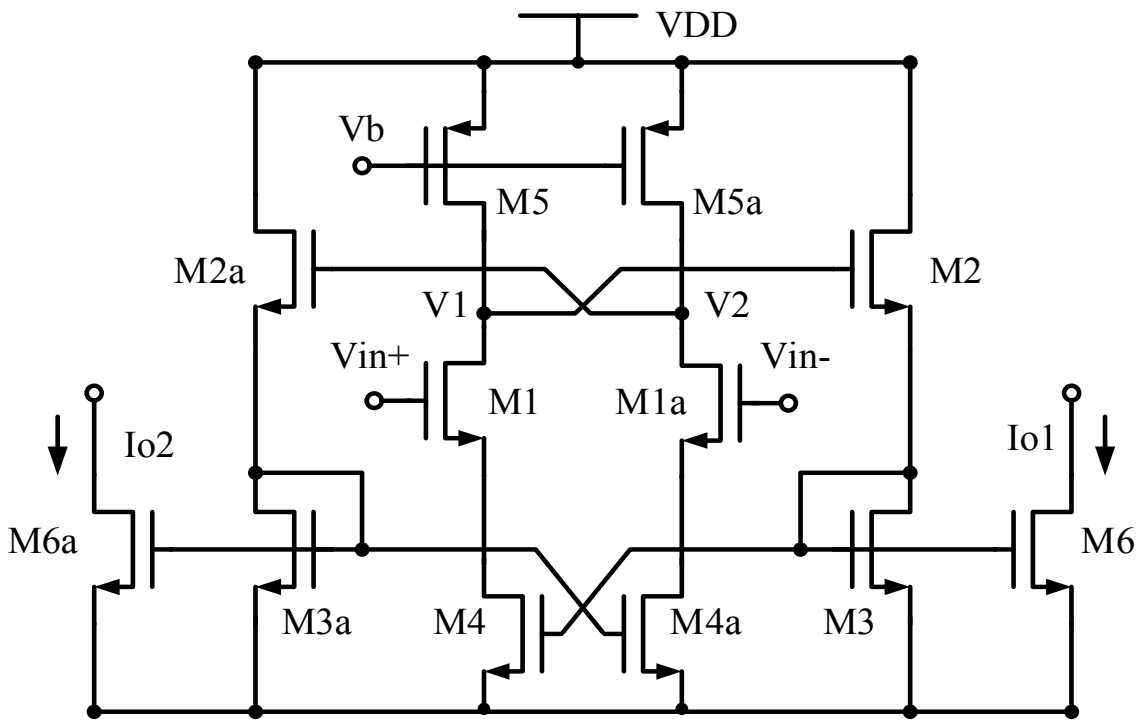


Fig. 1.11 The rail-to-rail Gm amplifier

### (c) Conventional Gm amplifier

To solve the problem of Gm value that changed by process variation, the conventional Gm amplifier shown in Fig. 1.12 is widely used [13]. It uses two voltage follow and a resistor to transfer the input voltage into output current we want. From Fig. 1.12, we can find the Gm value is  $\frac{1}{R_G}$ . Once we replace  $R_G$  by MOS resistor, we can

tune the Gm value by the gate voltage of the MOS resistor. Although we solve the problem of imprecise Gm value caused by process variation, there is another problem of this kind of Gm amplifier.

Because we always put a resistor at the input stage which is a voltage follow, the resistor's value will affect the gain of the source follow. Once we put a small  $R_G$  at the source of the MOS, we will not have a unity gain of source follow.



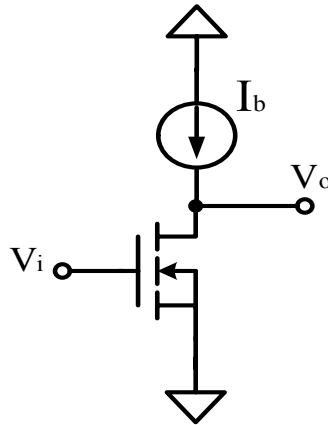


Fig. 1.13 Common-drain amplifier (voltage follower)

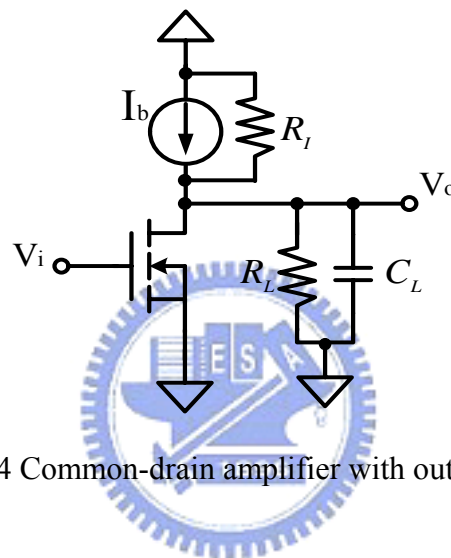


Fig. 1.14 Common-drain amplifier with output loads

### 1.3 MOTIVATION

The electrophysiological signals of human body are very small and the frequency is low. The common voltage range is from 50 micro volts for the brain wave (EEG) to 5 mV for some heart voltage (ECG). This rarely goes down to 0.5 micro volts for evoked potential like retina voltage (ENG) or hearing hair cell to the brain stem audio nerve voltage. Besides, the frequency range is usually low, no more than 2 KHz for most cases and seldom extended to 40 KHz.

Besides, there are a lot of low frequency noises in the human body. The frequency of these noises overlaps the frequency range of human body signals. Therefore, the most important part of the front-end portable system is the instrumentation amplifier (INA).

We use the INA to compress the noises and amplify the electrophysiological signals we need. So we have to design a high common-mode rejection ratio (CMRR) instrumentation amplifier which is the first stage of the portable system. Another point is that once our signal is very small, input offsets voltage and input noise play an important role in our instrumentation amplifier. Once the input offset voltage or input-referred noises become higher than the signals, we will not get any output signals.

Behind the instrumentation amplifier is the low-frequency bandpass filter to filter the signals we want. Human body signals are very low frequency (about 50Hz to 2 kHz), and the bandpass filter needs very large capacitors or resistors. It will increase the difficulty for put the large devices on chip or increase the size of the chip and the costs. To overcome this problem, we use some method in the thesis without using large devices.

Another problem is about the power of the circuits. Like most of the mobile systems, we need a low power design to make it more convenient to be portable. So the low power is another design consideration.

#### **1.4 THESIS ORGANIZATION**

This thesis contains four chapters. Chapter1 introduces the background of nursing system and remote medical care. Besides, the structure and function of the front-end circuit of the electrophysiological signals measurement system are also mentioned. At the end of Chapter1, some architectures of instrumentation amplifier which are already proposed to archive high CMRR will be described. Also the new architecture design of INA and low frequency filter of this thesis are presented. In Chapter2, we'll describe the circuits to construct the INA and the low frequency bandpass filter. Chapter3 shows the

simulation results of the front-end circuit of the electrophysiological signals measurement system. Finally, chapter4 describes the conclusion and future work.



## CHAPTER 2

### ARCHITECTURE AND CIRCUITS DESIGN

---

#### 2.1 ARCHITECTURE DESIGN OF THE INSTRUMENTATION AMPLIFIER

##### 2.1.1 Differential Difference operational amplifier (DDA)

Differential difference operational amplifier (DDA) is the extension concept of the differential operational amplifier. Its expression is showed in Fig. 2.1 and the difference between opamp and DDA is that instead of two single-ended inputs as in the case of op-amps, it has two differential input ports  $(V_2 - V_1)$  and  $(V_4 - V_3)$ . The output voltage of the DDA can be written as:

$$V_o = A_o [(V_4 - V_3) - (V_2 - V_1)] \quad (2-1)$$

$A_o$  is the open-loop gain of the DDA. When a negative feedback is introduced to  $V_1$  or  $V_4$ , the basic equation that characterizes the operation of the DDA is obtained as :

$$V_2 - V_1 = V_4 - V_3 \quad (2-2)$$

when  $A_o \rightarrow \infty$

The DDA is a widely used block in many circuit applications because it has four inputs to have more function changing.

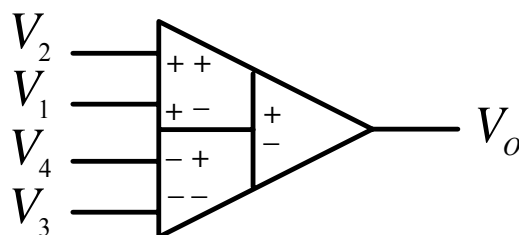


Fig. 2.1 The symbol for Differential Difference Operational Amplifier

## 2.1.2 Differential Difference operational transconductance amplifier (DDGm)

Like the differential difference operational amplifier which is extended from operational amplifier, differential difference operational transconductance amplifier (DDGm) is extended from operational transconductance amplifier. Fig. 2.2 is the expression of DDGm and its function is:

$$I_o = G_m [(V_4 - V_3) - (V_2 - V_1)] \quad (2-3)$$

$G_m$  is the transconductance

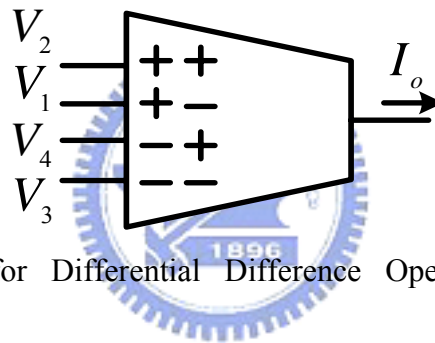


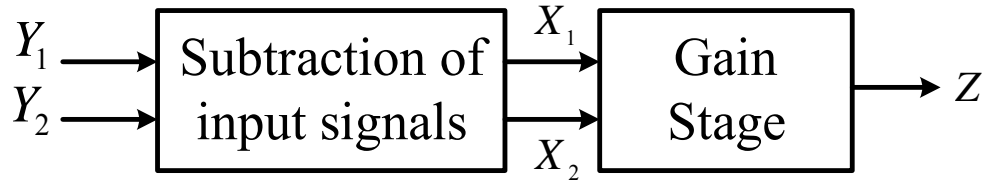
Fig. 2.2 The symbol for Differential Difference Operational Transconductance Amplifier

When the output has a resistor loading, we can obtain the same function (2-2). The differential difference operational transconductance amplifier also has multiple functions and we'll use the DDGm in our new structure of instrumentation amplifier.

## 2.1.3 New structure design of the instrumentation amplifier

We have introduced some structures of instrumentation amplifiers in chapter1; most of the structures transfer the voltages of input signals into current in the first stage. Then they amplify the current and subtract the current in the second stage. If we can do

the action of current transformation and the subtraction of the input signals simultaneously at the first stage then amplify the signals at the second stage, the common mode signals will be compressed twice. Fig. 2.3 shows the structure of this idea.



$$\begin{cases} Y_1 \text{ (sine)} - Y_2 \text{ (sine)} = X_1 \text{ (flat)} (V_{cm}) \\ Y_1 \text{ (sine)} - Y_2 \text{ (inverted sine)} = X_2 \text{ (double sine)} (2V_d) \end{cases}$$

Fig. 2.3 Expression for the new approach of instrumentation amplifier

As showed in Fig. 2.3, we subtract input signals in the first stage and the noises (common-mode signals) will almost equals to zero with differential signals become double. As a result, before entering the gain stage, the noises have been eliminated and the gain stage also has the ability to compress common-mode signals. Under this structure, common mode rejection ratio would be high.

The function of the idea for first stage can be realized by our new circuit – differential difference operational transconductance amplifier. Once we connect the differential difference operational transconductance amplifier like Fig. 2.4, we can get the output signal as:

$$\begin{aligned} I_o &= G_m [(V_{ref} - V_o) - (V_1 - V_2)] \\ \Rightarrow \frac{V_o}{R_a} &= -G_m V_o + G_m V_{ref} - G_m \Delta V_{in} \\ \Rightarrow V_o (1 + G_m R_a) &= G_m (V_{ref} - \Delta V_{in}) \end{aligned}$$



$$V_o = \frac{G_m R_a}{1 - G_m R_a} (V_1 - V_2 - V_{ref})$$

$$\approx (\Delta V_{in} - V_{ref}) \quad (2.3)$$

And we can get a voltage subtraction function using this method to cancel the common-mode signals.

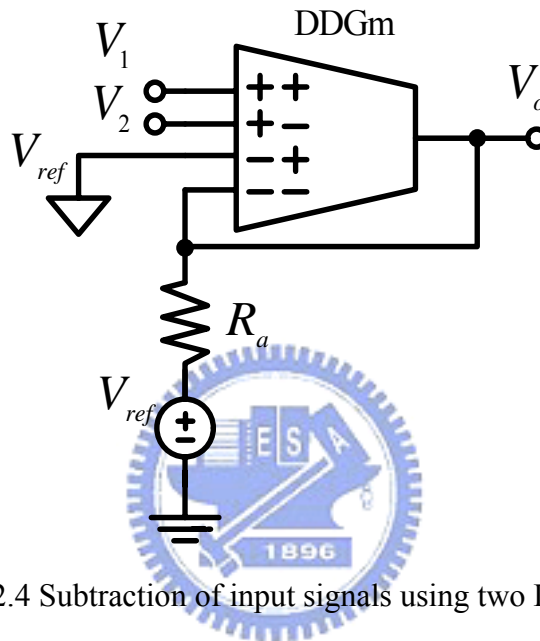


Fig. 2.4 Subtraction of input signals using two DDGm

After using the function showed in equation (2.3), we can design a new structure of high CMRR instrumentation amplifier. Fig. 2.5 is the structure of the new high CMRR INA using DDGm. The main function of the first stage is to cancel the common-mode and doubles the differential signal like Fig. 2.6 showed. Briefly speaking, we can say that the first stage constructed with two DDGm is to enhance the differential signal and to compress the common-mode signals (noises). Then the second stage with Gm amplifier and  $R_G$  is to provide the gain for signals. Equation (2.4) derives the node voltage of  $V_{x1}$  and  $V_{x2}$ .

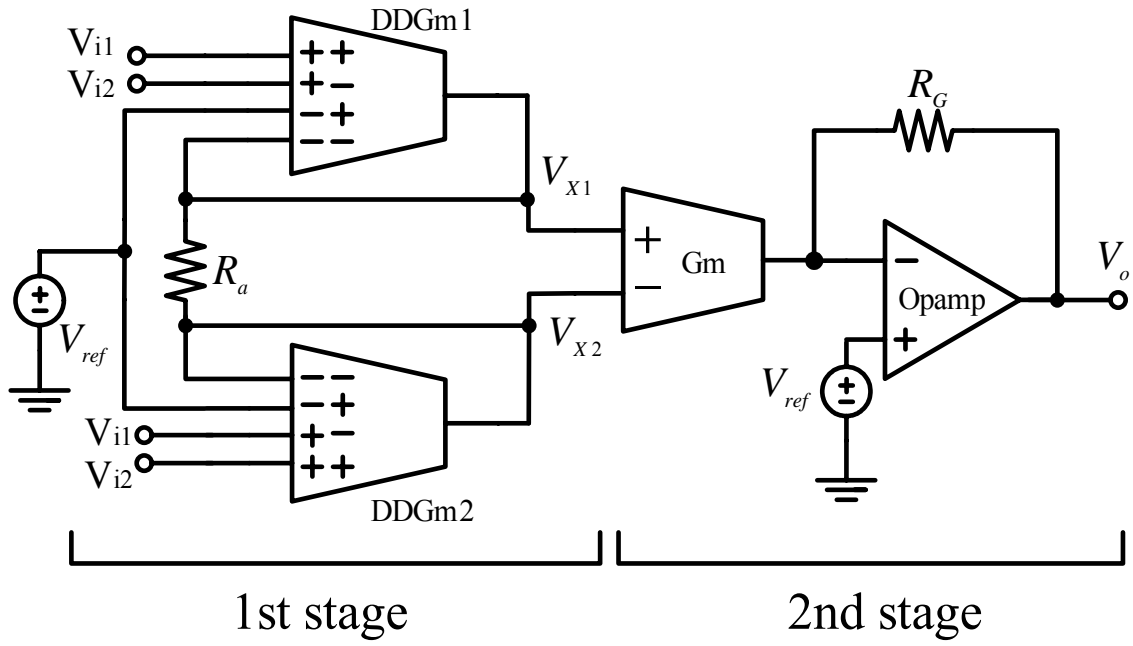


Fig. 2.5 The new structure of high CMRR instrumentation amplifier

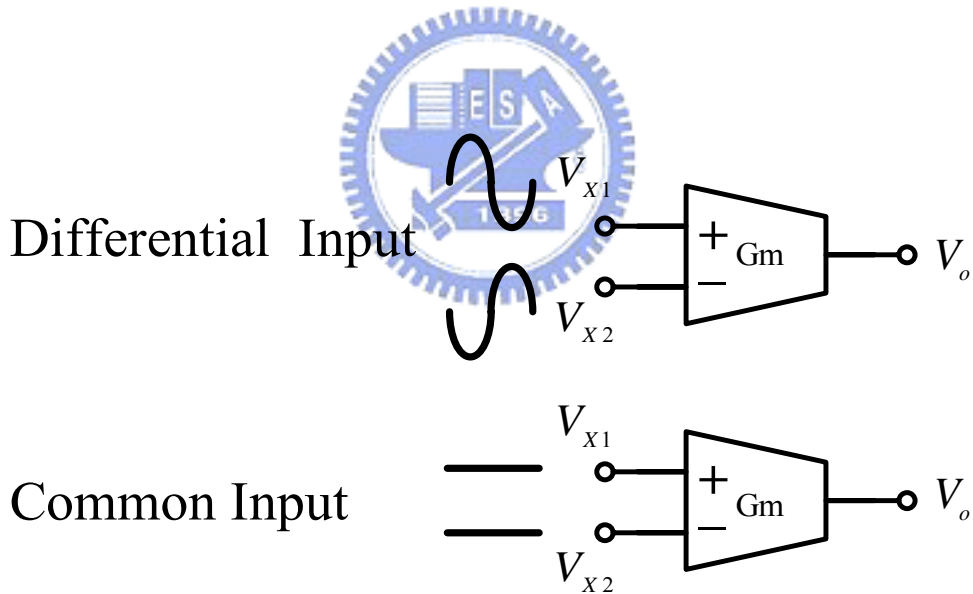


Fig. 2.6 The function of the first stage and waveform of  $V_{X1}$  and  $V_{X2}$

$$V_{X1,dm} = V_{i1,dm} - V_{i2,dm} = 2V_{dm}$$

$$V_{X2,dm} = V_{i2,dm} - V_{i1,dm} = -2V_{dm}$$

$$V_{X2,cm} = V_{i2,cm} - V_{i1,cm} \approx 0$$

$$V_{X1,cm} = V_{i1,cm} - V_{i2,cm} \approx 0$$

(2.4)

## 2.2 CIRCUIT DESIGN OF THE DIFFERENTIAL DIFFERENCE OPERATIONAL TRANSCONDUCTANCE AMPLIFIER

### 2.2.1 The Flipped Voltage Follower (FVF)

The most commonly used voltage follower is shown as Fig. 1.13. It is widely used in many operational amplifiers for voltage buffer and input stage for operational transconductance amplifier like Fig. 1.12. This voltage follower is also used in many analog circuits. However, it has a drawback that would influence the performance of the analog circuits.

To solve this problem, the paper [14] claimed a new voltage follower circuit called flipped voltage follower (FVF) shown in Fig. 2.7. In Fig. 2.7 the current through M1 is held constant and independent on the output current. It could be described as a voltage follower with shunt feedback. Neglecting body effect and the short-channel effect,  $V_{SGM1}$  is held constant, and voltage gain is unity. Unlike the conventional voltage follower, FVF is able to source a large amount of current, but its sinking capability is limited by the biasing current  $I_b$ . The large sourcing capability is due to the low impedance at the output node, which is approximately  $r_o = \frac{1}{g_{m1}g_{m2}r_{o1}}$ , where  $g_{mi}$  and  $r_{oi}$  are the transconductance and output resistance of transistor, respectively. This value is in the order of 20-100  $\Omega$ .

And we will use this circuit to construct our differential difference operational transconductance amplifier.

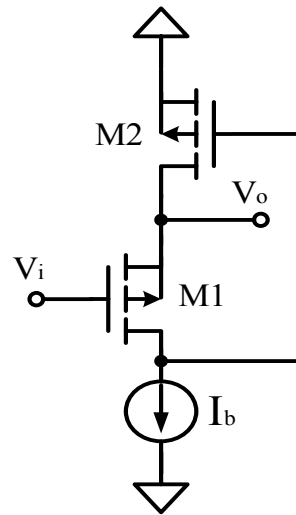


Fig. 2.7 Flipped Voltage Follower



## 2.2.2 The differential difference operational transconductance amplifier

Using the flipped voltage follower (FVF), we can design a DDGm circuit shown in Fig. 3.8. The magnitude of  $G_m$  can be derived as follow:

$$\begin{aligned}
 V_{x1} &= \frac{V_{i1} + V_{i2}}{2}, \quad V_{x2} = \frac{V_{i3} + V_{i4}}{2} \\
 \Rightarrow V_{x1} - V_{x2} &= \frac{V_{i1} + V_{i2} - (V_{i3} + V_{i4})}{2} \\
 \Rightarrow I_o &= \frac{(V_{i1} - V_{i3}) - (V_{i4} - V_{i2})}{2R_m} \\
 \Rightarrow G_m &= \frac{1}{2R_m} \tag{2.4}
 \end{aligned}$$

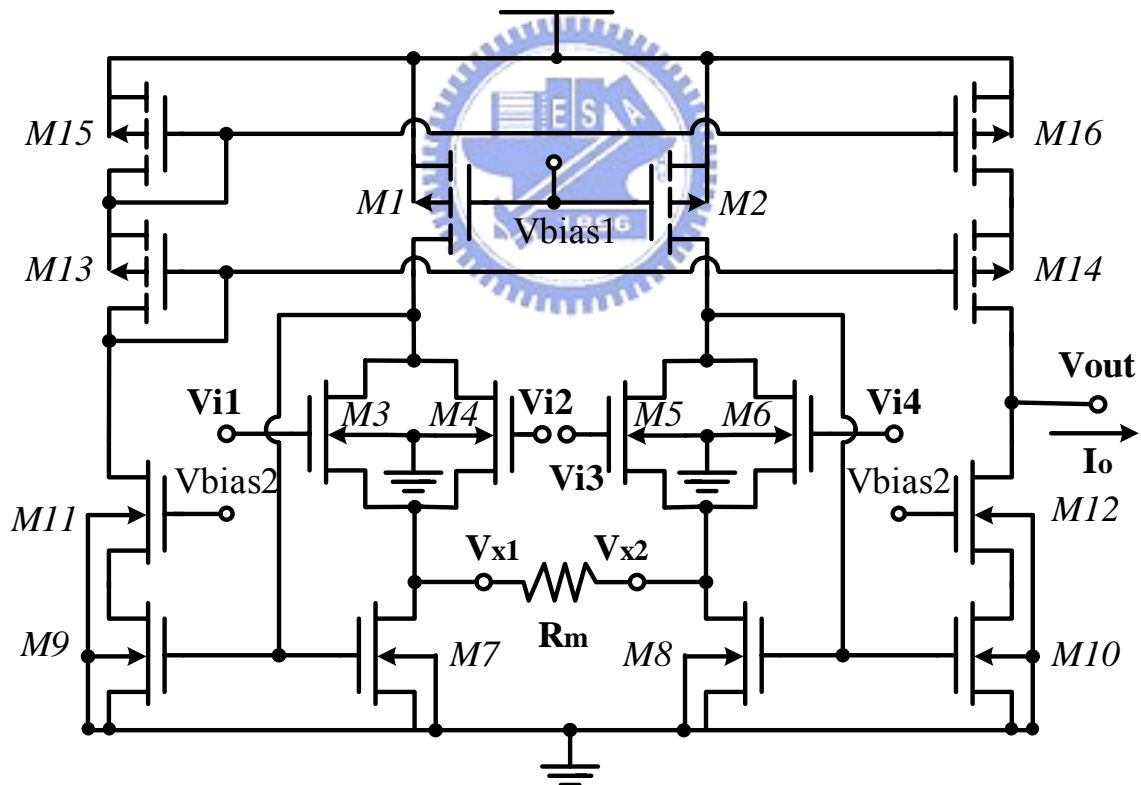


Fig. 2.8 The DDGm amplifier using FVF method

In Fig. 2.8,  $M13 \sim M16$  are the cascode current mirror. The stacked MOS can decrease the channel length effect of and enhance the accuracy of the mirrored current

ratio. On the other hand, the output resistance of an ideal transconductance amplifier is infinite, so the stacked MOS  $M9 \sim M16$  can increase  $r_o$  of the DDGm circuit.

<b>MOS</b>	<b>size</b>	<b>m</b>
$M1 \ 、 M2$	(0.5/10)	10
$M3 \ 、 M4 \ 、 M5 \ 、 M6$	(0.5/10)	1
$M7 \ 、 M8$	(0.7/10)	1
$M9 \ 、 M10$	(0.4/9)	1
$M11 \ 、 M12$	(0.4/4)	1
$M13 \ 、 M14$	(1/4.2)	3
$M15 \ 、 M16$	(1/4)	5

Table 2.1 The size of the DDGm amplifier in Fig. 2.10

## 2.3 STRUCTURE DESIGN OF THE LOW-FREQUENCY BANDPASS FILTER

### 2.3.1 Specification of the low-frequency bandpass filter

For the electrophysiological measurement system, we can set the spec of the low-frequency bandpass filter as Table 2.2.

From the Table 2.2, we can find the frequency range is from 50 Hz to 2 kHz, the stopband attenuation is about 35 to 40 dB, and the passband ripple is from 3 to 8dB. From the spec we set, we can use the Inverse Chebyshev or the Elliptic filter to realize it. By the comparison of the two LC networks of Inverse Chebyshev and the Elliptic filter we derived, we can find that the element values of Elliptic filter is much more realizable than the f Inverse Chebyshev filter. So finally, we choose the 5th-order Elliptic filter structure to design our desired low-frequency bandpass filter.

<b>Filter Spec</b>	
Low corner frequency	50 Hz
High corner frequency	2 kHz
Stop band ratio	1.98
Stop band attenuation	35~40 dB
Pass Band Ripple	3~10 dB
Gain	>0dB
Type of the Filter	5th order Elliptic

Table 2.2 The specification of the low-frequency bandpass filter

### 2.3.2 LC network and the leapfrog structure

From the spec of Table 2.1, we can derive the transfer function of the low-frequency bandpass filter showed in equation (2.5). And from equation (2.5), we can derive the LC network in Fig. 2.9. In Fig. 2.9, we can find that the element values of the capacitors won't be able to be realized on the integrated circuits. So we have to scale the element values of Fig. 2.9 into the values that can be made on chip reasonable. Fig. 2.9(b) is the circuit after normalizing the element values from Fig. 2.9 (a); we make all the capacitor values from 0.1pF to 10pF using the normalization method of equation (2.6) and (2.7).

$$\frac{677 \cdot S^5 + (5.184)^{11} \cdot S^3 + (1.055)^{16} \cdot S}{S^6 + 7241 \cdot S^5 + (1.544)^8 \cdot S^4 + (5.702)^{11} \cdot S^3 + (6.095)^{14} \cdot S^2 + (1.128)^{17} \cdot S + (6.151)^{19}} \quad (2.5)$$

$$C' = \frac{C}{\sqrt{R_S \cdot R_L}} \quad (2.6)$$

$$L' = L \cdot \sqrt{R_S \cdot R_L} \quad (2.7)$$

As we mentioned before, we'll use the leapfrog structure to decrease the effects of

variations for element values. Leapfrog structure uses the feedback topology, so the performance of the filter will be less sensitive to the variation of the element values. For leapfrog structure, we change the position of the elements in Fig. 2.9(b) into the Fig. 2.9(a) to make more blocks showed in Fig. 2.10(b).

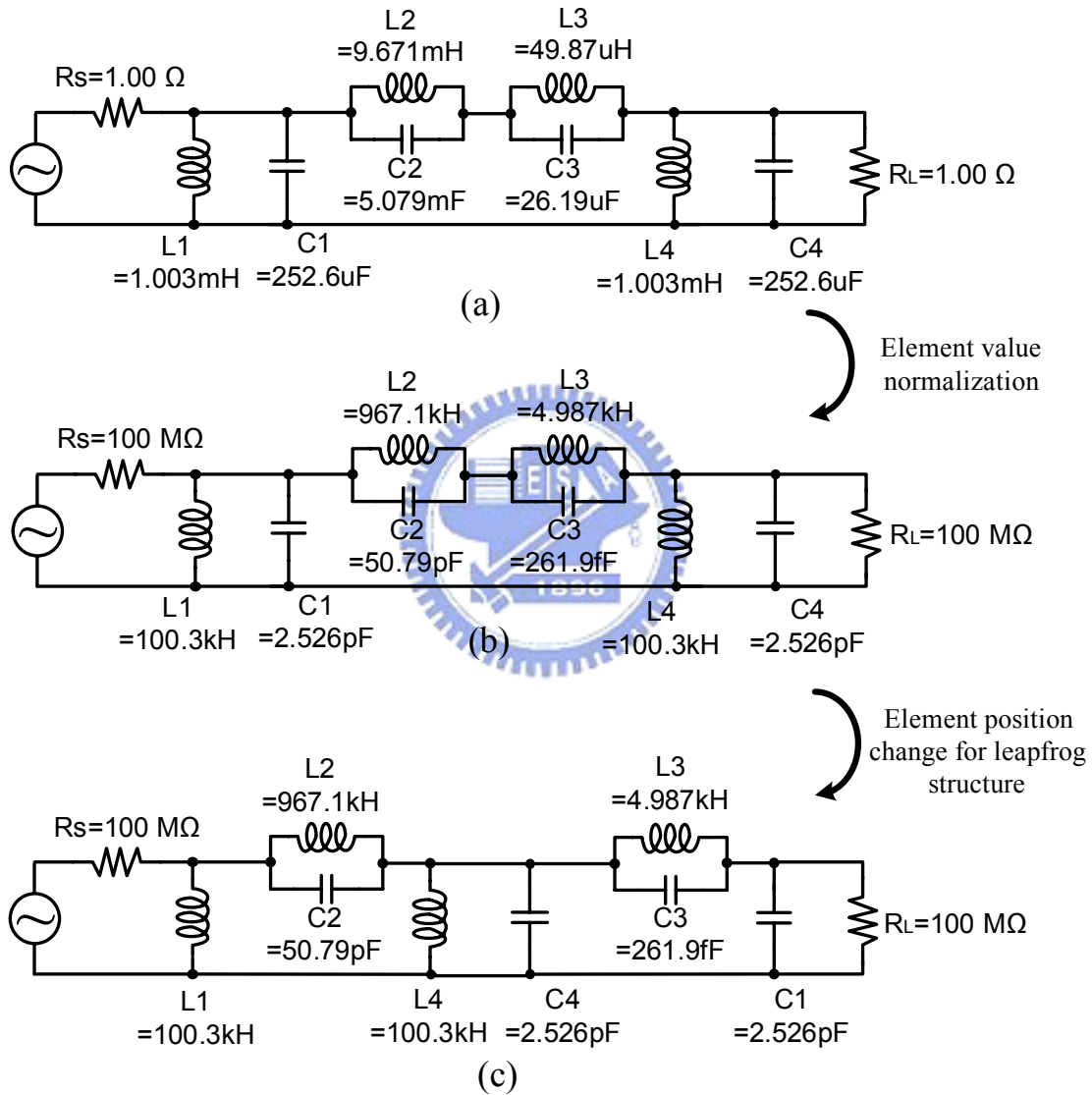


Fig. 2.9 (a) The prototype LC network of the 5th-order Elliptic bandpass filter  
 (b) The LC network after element value normalization.  
 (c) The LC network after element position change for leapfrog structure



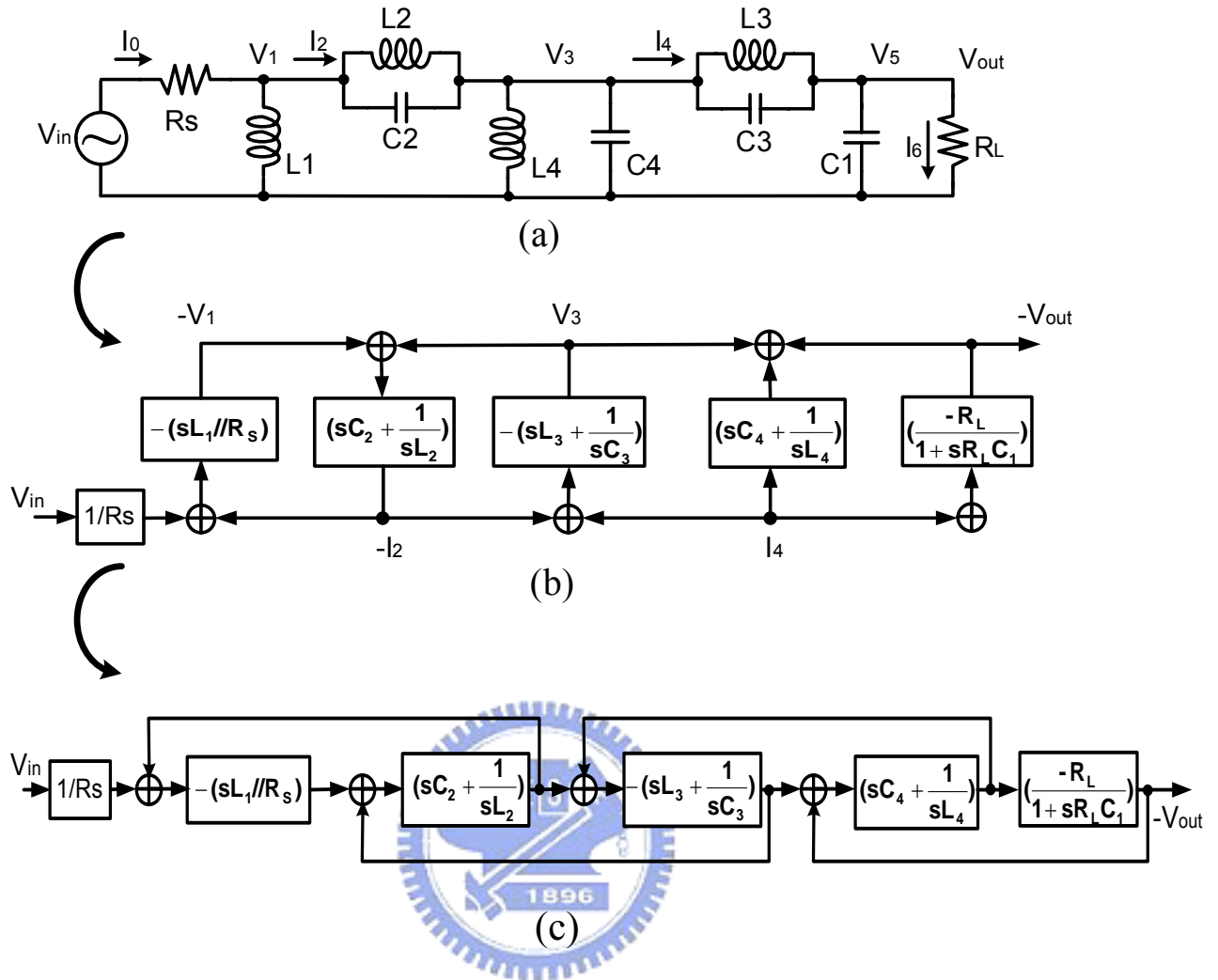


Fig. 2.10 (a) The LC network of the 5th-order BP Elliptic filter

(b) The block diagram of leapfrog structure for the 5th-order BP Elliptic filter

(c) The block diagram of leapfrog structure for the 5th-order BP Elliptic filter

The Fig. 2.10 (a) (b) (c) shows the procedure of how to transfer LC network into leapfrog structure. It is obvious to see that in each block diagram that the loops consists of an inverting and a noninverting block so that the gain around each loop is negative as required for stability. Also from the Fig. 2.10 (a) (b) (c), we can now understand that why we have to change the element position in Fig. 2.9(b) into Fig. 2.9(c). This action not only increases the block diagram but decentralize the elements so we can gain more stability of the filter.

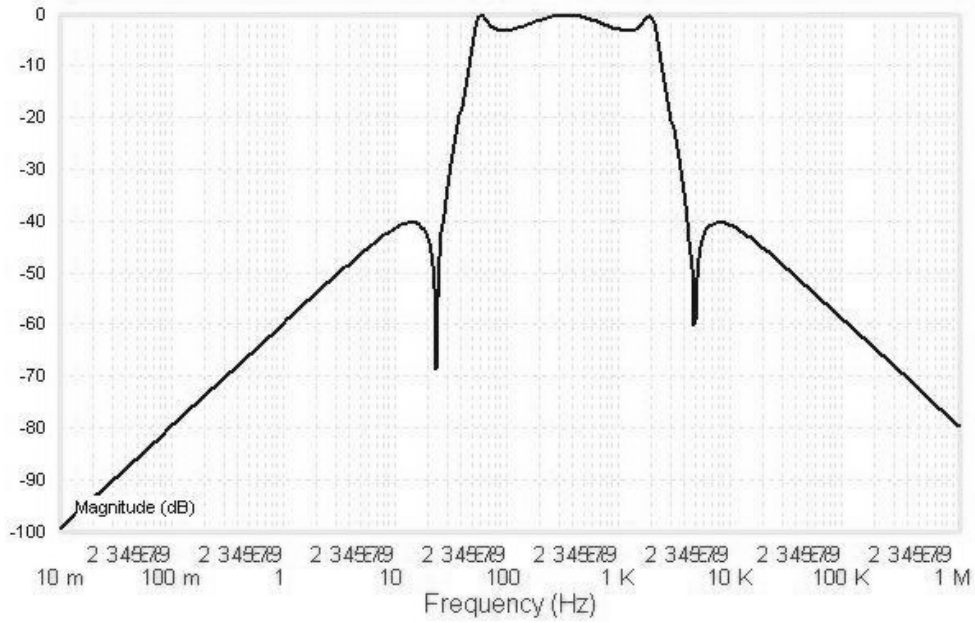


Fig. 2.11 The simulation result of 5<sup>th</sup>–order Elliptic LC ladder

Fig. 2.11 shows the simulation result of the 5<sup>th</sup>–order bandpass Elliptic filter by the LC ladder in Fig. 2.9(c). We can find the ripple in both the passband and stopband as we discussed in chapter 1.2. In the next section, we'll transfer the LC ladder into leapfrog structure and Gm-C filter.

### 2.3.3 Gm-C filter

After deciding the block diagram of the leapfrog structure, it's time to decide the actual implementation of the circuit. Fig. 2.12 shows how to realize the blocks in Fig. 2.10(b).

	Circuit	Function
a		$\frac{1}{sC} \cdot \frac{1}{R_N} = \frac{G_m}{sC}$
b		$G_m \left( sL + \frac{1}{sC} \right)$ $= R_N \left( \frac{1}{sL'} + sC' \right)$
c		$\frac{G_{m0}/G_{m1}}{1 + \frac{sC}{G_{m1}}} = \frac{R_s/R_N}{1 + sR_s C'}$
d		$\frac{R_N}{R_s} = \frac{G_{m1}}{G_{m1} + G_{m2}}$

Fig. 2.12 Circuits implementations for functions of the functions in Fig. 2.10

In Fig. 2.12,  $R_N$  is the normalize factor and  $R_s$  is the  $R_s$  in Fig. 2.10(c); therefore we can realize the different function shown in Fig. 2.10(c). Back to Fig. 2.10, we can find the value of the inductors is hard to implement on an integrated circuit. To solve this problem, we have to replace the passive inductors with some active circuits. A two-port network is shown in Fig. 2.13, we call this kind of structure “Gyrator” which is composed of transconductance amplifiers and impedance loading. So we can realize the passive inductor into an “active” inductor by transconductance amplifiers and capacitors.



Fig. 2.13 The two port network of Gyrator

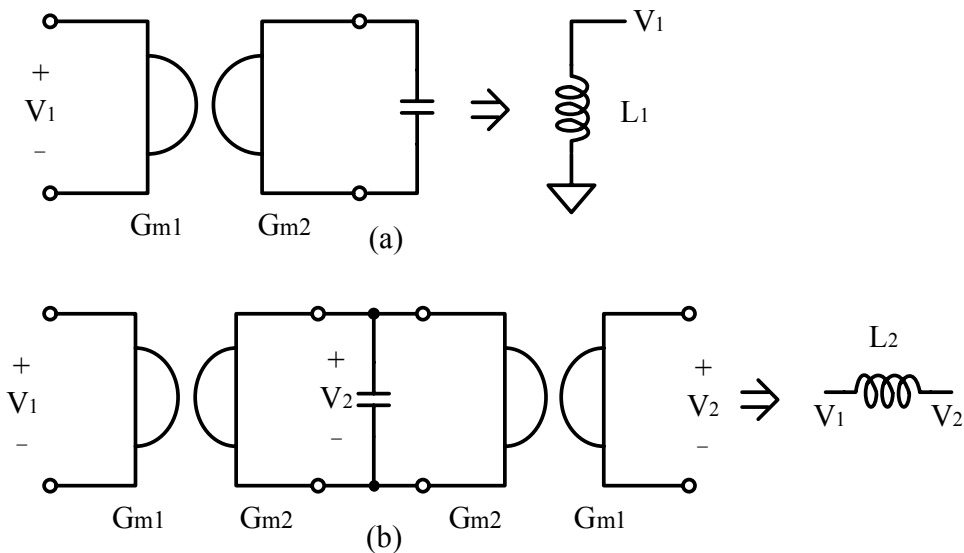


Fig. 2.14 (a) The realization of a grounded inductor

(b) The realization of a floating inductor

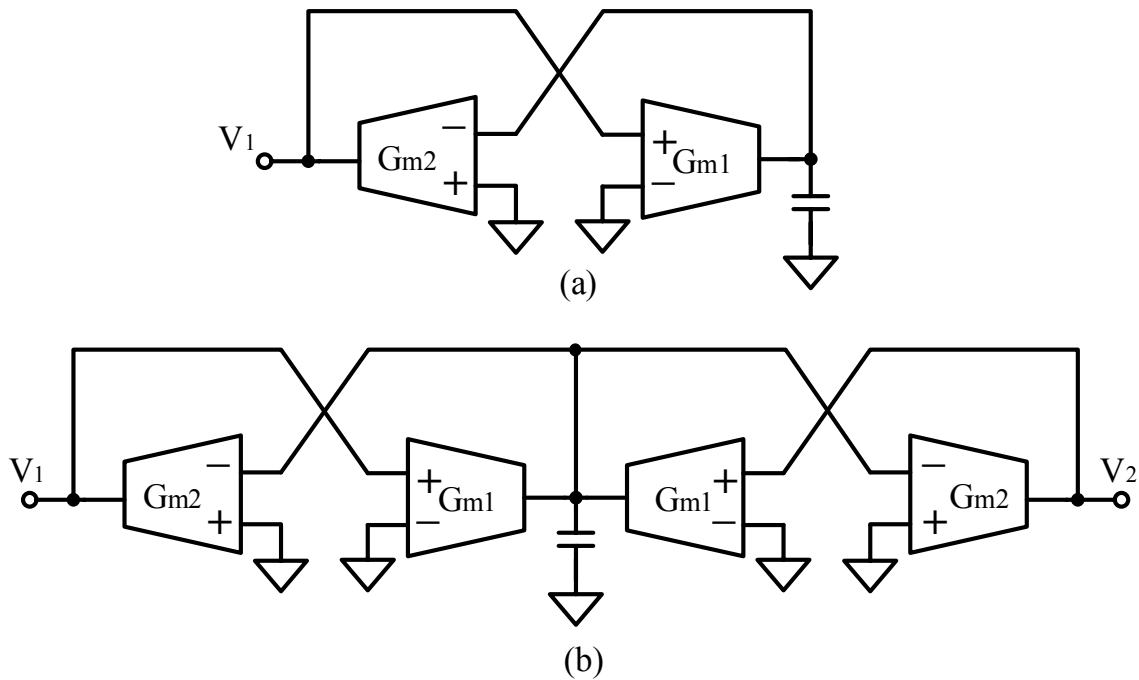


Fig. 2.15 (a) The realization of a grounded inductor composed of Gm and capacitor

(b) The realization of a floating inductor composed of Gm and capacitor

$$L = \frac{C}{G_{m1} \cdot G_{m2}} \quad (2.8)$$

Fig. 2.14(a) and Fig. 2.14(b) are the Gyrator of grounded and floating inductors shown in two-port networks. Fig. 2.15(a) and Fig. 2.15(b) are the Gyrator composed of Gm amplifier and capacitors. Equation (2.8) is the relation of the inductor, the Gm amplifier and the capacitor. Finally, from Fig. 2.10(c), Fig. 2.12 and Fig. 2.15 (a), we can derive the leapfrog Gm-C filter for low-frequency and bandpass Elliptic type.

Table 2.3 is the Gm values of the Gm-C filter. We can find the Gm value is very small, and the very small transconductance value is a little bit hard to realize because we need a huge resistor value to make a small transconductance. On the other hand, small Gm causes small current, so we have to eliminate the offset current of the Gm amplifier. In the following sections, we'll discuss some nonideal effects of the Gm amplifier when used in leapfrog filters.

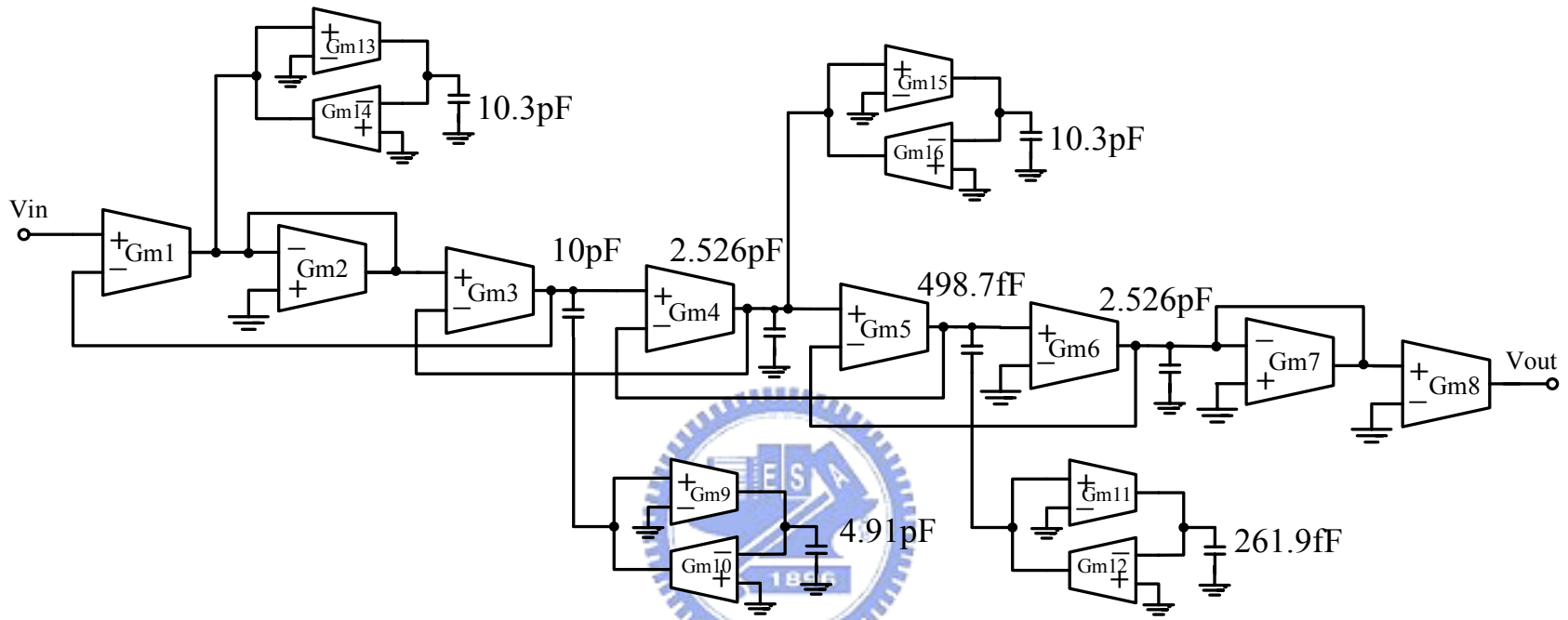


Fig. 2.16 The low-frequency bandpass Gm-C filter with leapfrog structure

Gm1 、 Gm4 、 Gm6 、 Gm8 、 Gm9 、 Gm10	<b>1nA/V</b>
Gm2 、 Gm3 、 Gm7 、 Gm11~Gm16	<b>10nA/V</b>
Gm5	<b>100nA/V</b>

Table 2.3 Gm values of the Gm amplifier in Fig. 2.17

## 2.4 CORE CIRCUIT DESIGN OF THE FILTER

### 2.4.1 The Gm amplifier using the mos resistor

As the shown in Fig. 2.16, the Gm value is from 1nA/V to 100nA/V which needs almost  $G\Omega$  scale resistor to have such Gm value. However, it's impossible to have passive resistors to  $G\Omega$  scale on integrated circuits. As a result, we need to have a mos resistor operated in the subthreshold region to get a  $G\Omega$  scale resistor. Fig. 2.17 shows the core circuit of the Gm amplifier and Table 2.3 shows its size. Fig. 2.18 is the Gm amplifier with mos resistor operated in subthreshold region. We use Vctrl in Fig. 2.18 to control the mos resistor value. Equation (2.10) is the equation of the mos current operated in subthreshold region and equation (2.11) is the slope of Vctrl versus Ids. The equation (2.9) is the Gm value derived and this equation includes the channel length modulation of M7 & M8

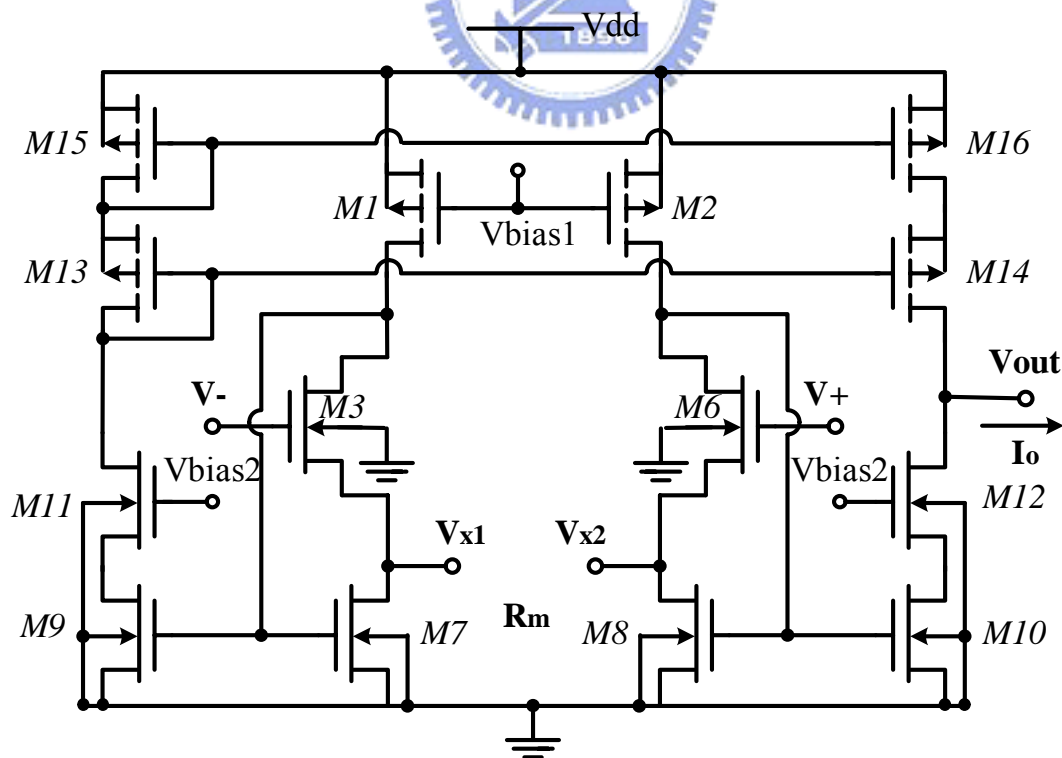


Fig. 2.17 The circuit of the Gm amplifier

MOS	size	m
$M1$ 、 $M2$	(0.5/10)	10
$M3$ 、 $M4$ 、 $M5$ 、 $M6$	(0.5/10)	1
$M7$ 、 $M8$	(0.7/10)	1
$M9$ 、 $M10$	(0.4/9)	1
$M11$ 、 $M12$	(0.4/4)	1
$M13$ 、 $M14$	(1/4.2)	3
$M15$ 、 $M16$	(1/4)	5

Table 2.4 The size of the DDGm amplifier in Fig. 2.10

$$\begin{aligned}
 I_o &= \left( \frac{2}{R_m} + 2\lambda \right) V_{id} \\
 \Rightarrow G_m &= \frac{2}{R_m} + 2\lambda \\
 \left[ \lambda &= \frac{1}{V_A} = -\frac{1}{L_{eff}} \left( \frac{dV_{DS}}{dX_d} \right) \right]
 \end{aligned} \tag{2.9}$$

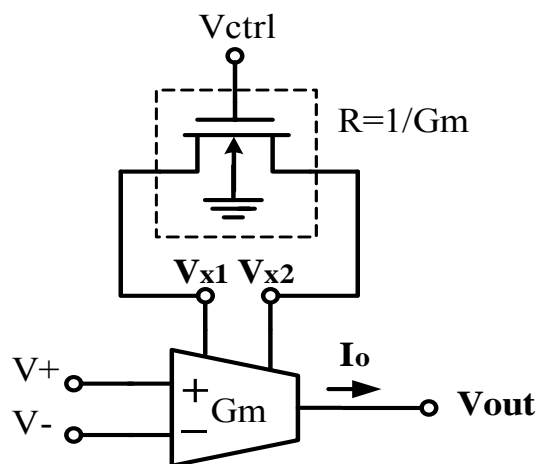


Fig. 2.18 The circuit of the Gm amplifier connected with MOS resistor



$$I_{ds} = \mu_{eff} C_{ox} \frac{W}{L} (m-1) \left( \frac{kT}{q} \right)^2 e^{q(V_g - V_t)/mkT} (1 - e^{-qV_{ds}/kT}) \quad (2.10)$$

$$S = \left( \frac{d(\log_{10} I_{ds})}{dV_g} \right)^{-1} = 2.3 \frac{mkT}{q} = 2.3 \frac{kT}{q} \left( 1 + \frac{C_{dm}}{C_{ox}} \right) \quad (2.11)$$

## 2.4.2 THE NONIDEAL EFFECTS OF THE GM AMPLIFIERS

When we simulate the low-frequency bandpass Elliptic filter with ideal Gm amplifiers with high output impedance and infinite bandwidth, we'll have a perfect simulation result of the filter. However, once we put the realistic Gm amplifier into the Elliptic filter, some nonideal effects of the Gm amplifier appears. These nonideal effects will affect the performance of the filter a lot. We'll discuss these effects in the following sections.



### (a) Background current

The Gm amplifier we use is the circuit in Fig. 2.17 with a mos resistor connected at nodes Vx1 and Vx2 and we use Vctrl in Fig. 2.18 to control the Gm value. Although we can get small Gm value through the mos resistor operated in subthreshold region, what if the “gm” of the circuit in Fig. 2.16 itself larger than the Gm we want? Once this happen, we will never get the small Gm no matter how large the resistor value is. This current we don't want is called the “background current “of our Gm amplifier.

Fortunately, we find a way to eliminate this background current. If we connect our Gm amplifier like Fig. 2.19, the background current won't flow forward to output. In Fig. 2.19, we connect the Gm amplifier's inputs in opposite way and connect the output together, then the background current will flow from the upper Gm amplifier with mos

resistor into the Gm amplifier below without mos resistor. After using this method, we can get the Gm value we want no matter how small it is.

However, the advantage of the way to eliminate background current will also increase our power of the Gm amplifier. For our electrophysiological signal measurement system, this would be a problem.

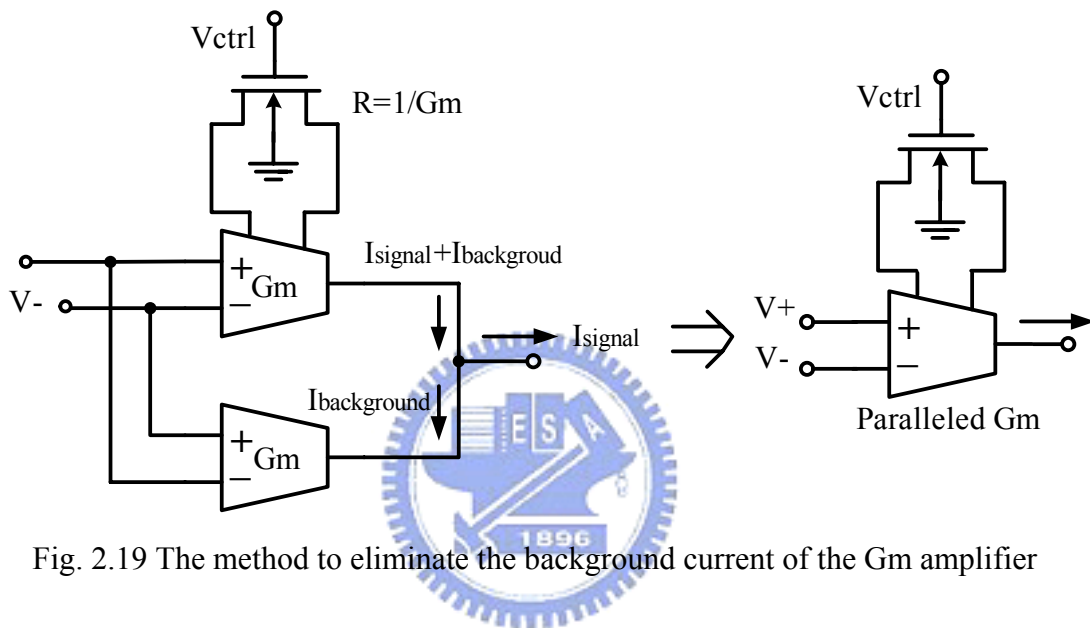


Fig. 2.19 The method to eliminate the background current of the Gm amplifier

### (b) Finite Ro effect in the Gyrator

We have introduced Gyrator in chapter 2.3, the ideal floating inductor for Gyrator is like 2.15(a). When we consider the finite output resistance of the Gm amplifier, we'll have a nonideal term compared to the equation (2.8). It is shown in Fig. 2.20 and derived as below:

$$\begin{aligned}
 Z &= \frac{1}{G_m^2} \times \frac{1+sRC}{R_o} \\
 &= \frac{1}{G_m^2} \times \frac{1}{R_o} + \frac{sC}{G_m^2}
 \end{aligned} \tag{2.12}$$

From equation (2.9) we can find that besides the imaginary part term “sL” we want, there will be a real part term  $R_s$ . Like the Q value of passive inductors, once we don't have enough output resistance of  $G_m$  amplifier, the frequency response of the LC tank at the resonant frequency will not be sharp enough.

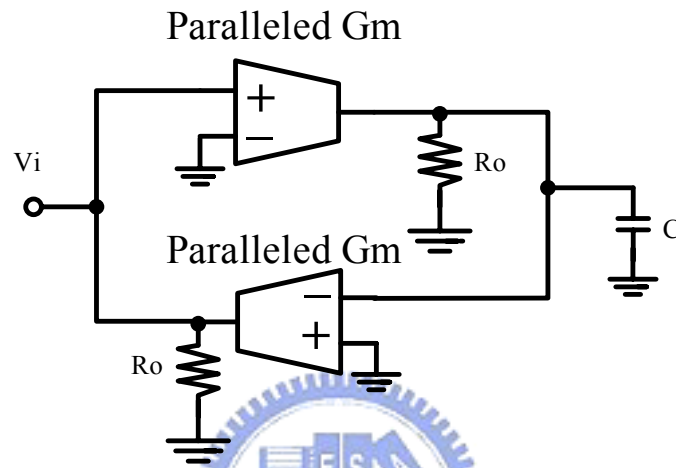


Fig. 2.20 The finite  $R_o$  of  $G_m$  amplifier in the Gyrator

**(c) Finite  $R_o$  and bandwidth limit of  $G_m$  amplifier in low-frequency filter design**

We have discussed the nonideal effect of Gyrator caused by the finite output resistance of  $G_m$  amplifier. Besides the Gyrator, output resistance not high enough will also bring serious problem in a low-frequency filter.

As showed in Fig. 2.21, if the output load of the  $G_m$  amplifier is a capacitor, the impedance of the capacitor is  $\left| \frac{1}{j\omega C} \right|$ . When the  $G_m$  amplifier is operated in low-frequency, the effect of finite output resistance appears. Suppose the input frequency is 1 kHz with a 1pF capacitor load at the output, the impedance of the capacitor is 0.16GΩ. Therefore, if we don't have enough output resistance, the current we want (the  $G_m$  we designed) will not totally flow into the capacitor. So we have to design a  $G_m$  amplifier with 5~10GΩ output impedance.

However, another question arises when we design a large output resistance of the Gm amplifier. That is when we have a large  $R_o$ , the dominant pole located at the output will be very small. For a filter whose passband is between 50~2 kHz, the bandwidth of the Gm amplifier should be at least 3kHz or above.

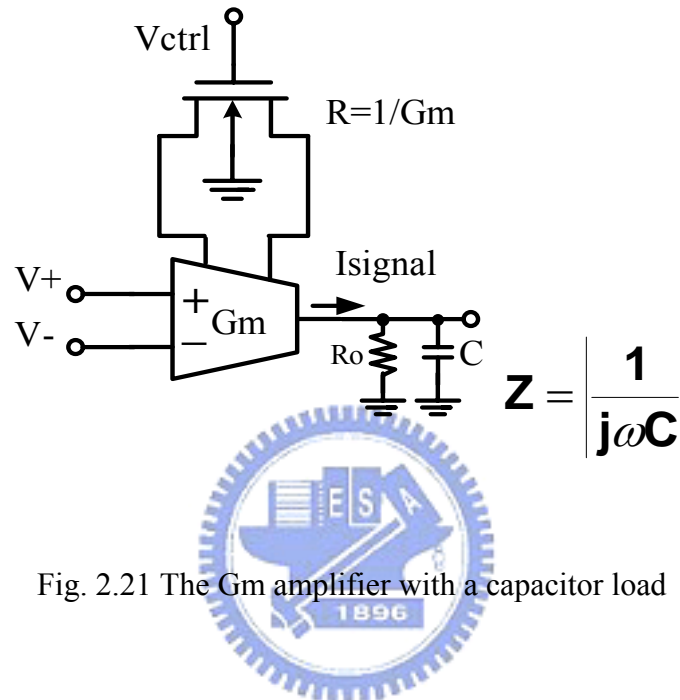


Fig. 2.21 The Gm amplifier with a capacitor load

Fig. 2.22 shows the ideal filter and the filter adding the nonideal effects of finite output resistance and too small bandwidth. The upper wave is the filter with infinite output resistance and bandwidth, and the below one is the filter with  $3G\Omega$  output resistance and 2.5 kHz bandwidth. In Fig. 2.22, the double-side narrow represents the gain decay caused by the infinite output resistance, and the circle represents the result with too small bandwidth.

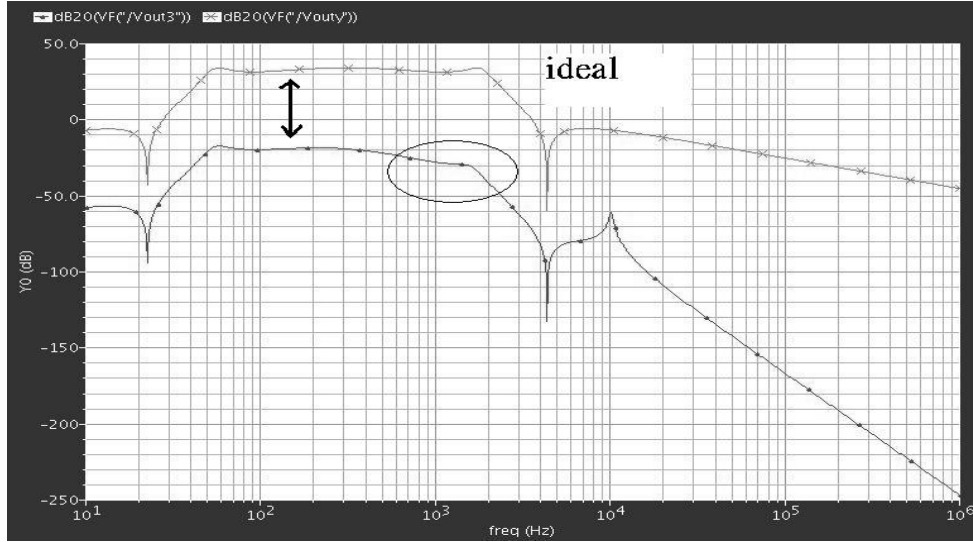


Fig. 2.22 The transfer function of the filter with ideal and nonideal Gm

Because of the tradeoff between Gm amplifier's output resistance and bandwidth, we have to do some optimize of the MOS sizes of the Gm amplifier in Fig. 2.17. And the output stage is showed in Fig. 2.23. Equation (2.13) derives the relation between Rout and the size of the output stage MOS and equation (2.14) shows the relation between 3dB frequency and the size of the output stage MOS.

$$\begin{aligned}
 R_{out} &= g_{m14} \cdot r_{o14} \cdot r_{o16} \\
 &\propto \sqrt{\frac{W_{14}}{L_{14}} \cdot I} \cdot \left(\frac{L_{14}}{I}\right) \cdot \left(\frac{L_{16}}{I}\right) = \frac{W^{\frac{1}{2}} \cdot L^{\frac{3}{2}}}{I^{\frac{3}{2}}} \\
 &= \frac{L^3}{W}
 \end{aligned} \tag{2.13}$$

$$\begin{aligned}
 RC &\propto \frac{W^{\frac{1}{2}} \cdot L^{\frac{3}{2}}}{I^{\frac{3}{2}}} \cdot W \cdot L = \frac{W^{\frac{3}{2}} \cdot L^{\frac{5}{2}}}{I^{\frac{3}{2}}} \\
 &= L^4 \\
 \rightarrow f_{3dB} &\propto \frac{1}{L^4}
 \end{aligned} \tag{2.14}$$

From equation (2.13) and (2.14), we can find that under the situation that the dc level of the Gm amplifier has been decided and the size of the MOS are scaled together, the Gm amplifier's  $R_{out}$  is proportional to  $\frac{L^3}{W}$  and  $f_{3dB}$  is proportional to  $\frac{1}{L^4}$ . From the conclusion we derived, we can find that when the W of the MOS are scaled,  $R_{out}$  would be scaled the same multiple and  $f_{3dB}$  won't change. As a result, we can design the W as minimum size. As regards to L, we can find that we can increase or decrease L neither because we won't gain both benefit in  $R_{out}$  or  $f_{3dB}$ . So we can just design our length to a middle value to ensure  $R_{out}$  and  $f_{3dB}$  are archiving the enough value.

$$\Rightarrow W \rightarrow \frac{W}{n} \Rightarrow \begin{cases} R_{out} \rightarrow n \cdot R_{out} \\ f_{3dB} = \text{constant} \end{cases}$$

$$L \rightarrow n \cdot L \Rightarrow \begin{cases} R_{out} \rightarrow n^3 \cdot R_{out} \\ f_{3dB} \rightarrow \frac{1}{n^4} \cdot f_{3dB} \end{cases} \quad (2.15)$$

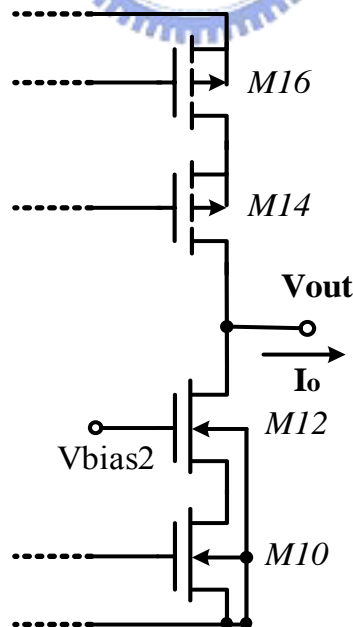


Fig. 2.23 The output stage of the Gm amplifier

## CHAPTER 3

### SIMULATION RESULTS

---

#### 3.1 SIMULATION RESULTS OF THE FLIPPED VOLTAGE FOLLOWER (FVF)

In chapter1 and chapter2, we have introduced the flipped voltage follower (FVF) which has the unity gain insensitive to output loads compared to the conventional voltage follower. And we have proved it in Fig. 3.1. We put different  $R_G$  from  $1k\Omega$  to  $100M\Omega$  at both the output of the FVF and conventional voltage follower. From Fig. 3.1, we can find that when  $R_G$  goes down from  $100M\Omega$  to  $5M\Omega$ , its gain degrades. And from  $5M\Omega$  to  $100k\Omega$ , the gain degrades more seriously. On the other side, the FVF will not degrade its gain until  $R_G$  goes down to  $500k\Omega$ . From the comparison in Fig. 3.1, the conclusion that FVF's gain is much more insensitive is proved.

Gain( $V_{out}/V_{in}$ )

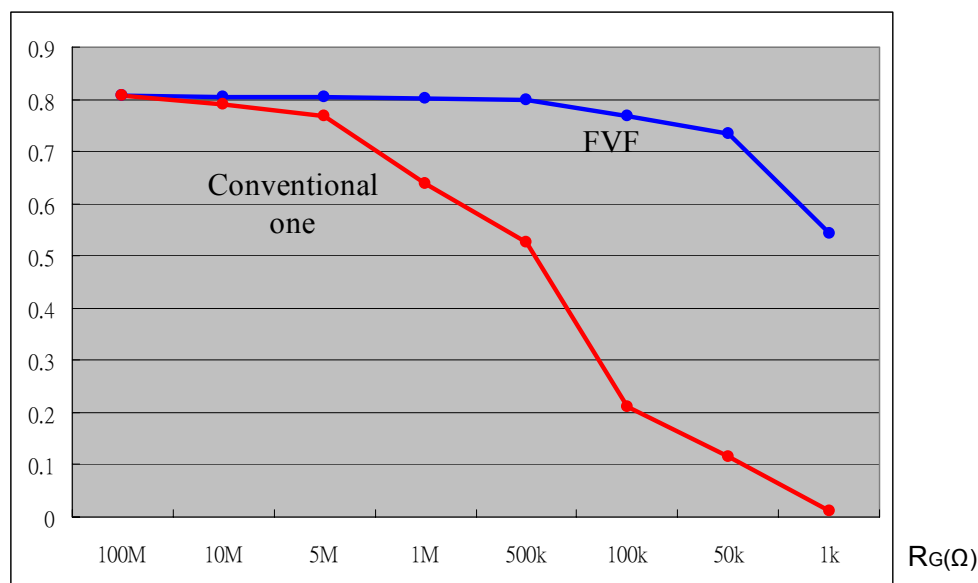


Fig. 3.1 The gain comparison of the conventional voltage follower and FVF versus  $R_G$

### 3.2 SIMULATION RESULTS OF THE GM AMPLIFIER

Fig. 3.2 shows the frequency response of Gm amplifier with different Gm values.

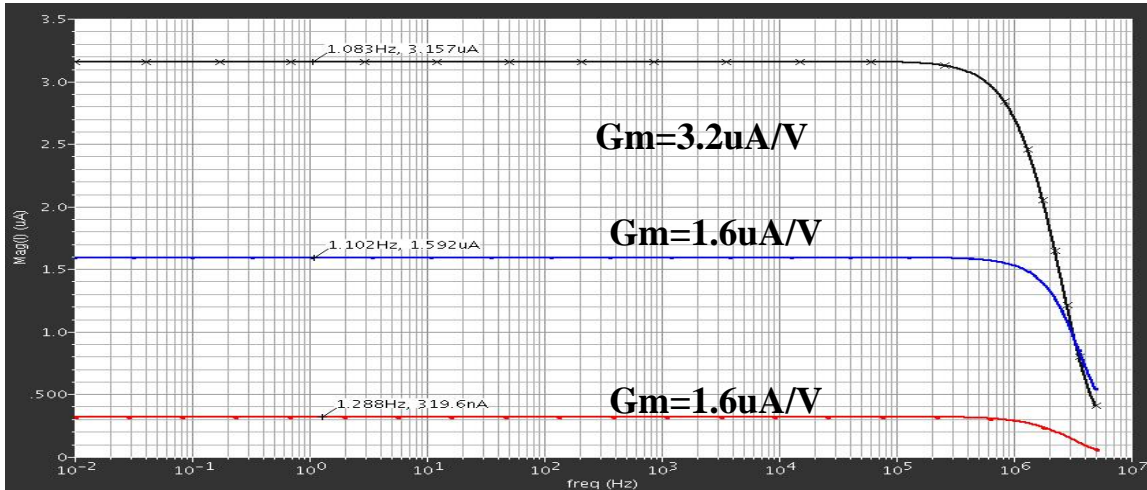


Fig. 3.2 The frequency response of the Gm amplifier with different Gm values

Fig. 3.3 shows the small Gm value that can achieve to 1.6 nA/V and 3.2 nA/V. It proves that we can successful eliminate the background current we discussed in chapter2.

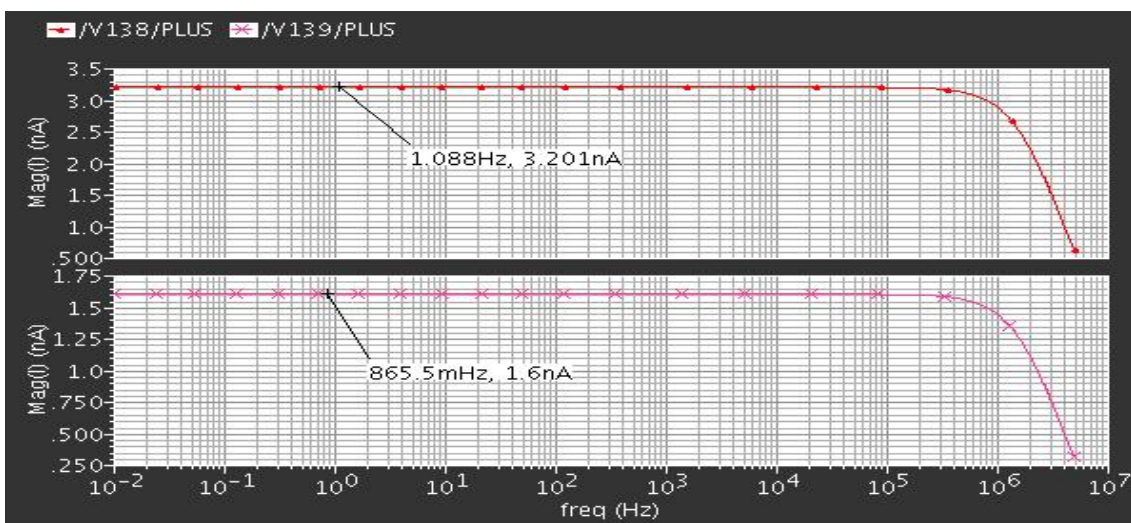


Fig. 3.3 The frequency response of the Gm amplifier with nA/V Gm values



In chapter2, we know the Gm value equals  $\frac{2}{R_m}$ . Now, we can prove that our output current after simulation almost equals to the current we calculate in theory in Fig. 3.4. We use different  $R_G$  from  $100\text{k}\Omega$  to  $1\text{G}\Omega$  and observe the output current. From Fig. 3.4, the HSPICE simulated current and the theoretical current are almost perfect matched.

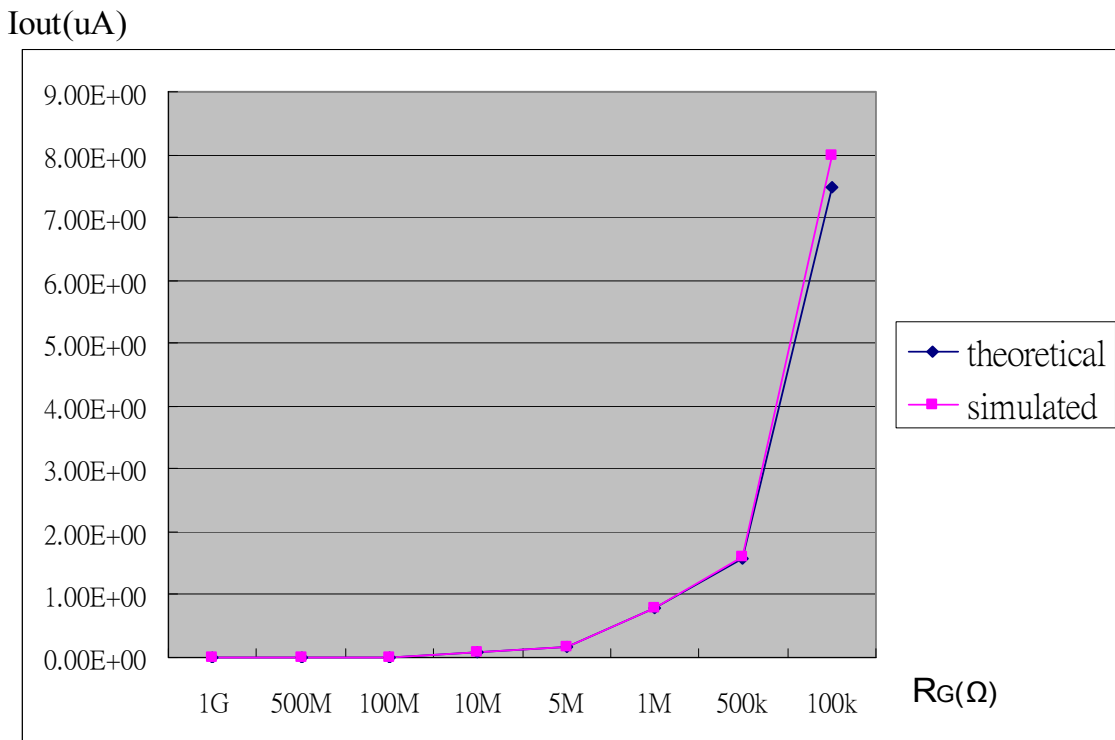


Fig. 3.4 The calculated and HSPICE simulated  $I_{out}$  versus  $R_G$

### 3.3 SIMULATION RESULTS OF THE INSTRUMENTATION AMPLIFIER

First, we have to test if the function of (2.3) and Fig. 2.4 works. If we input a differential signal whose amplitude is  $0.1\text{mV}$ , then we can find the amplitudes of node  $V_{x1}$  and  $V_{x2}$  (in Fig. 2.4) show in Fig. 3.5. From Fig. 3.5 we can find the amplitude is doubled.

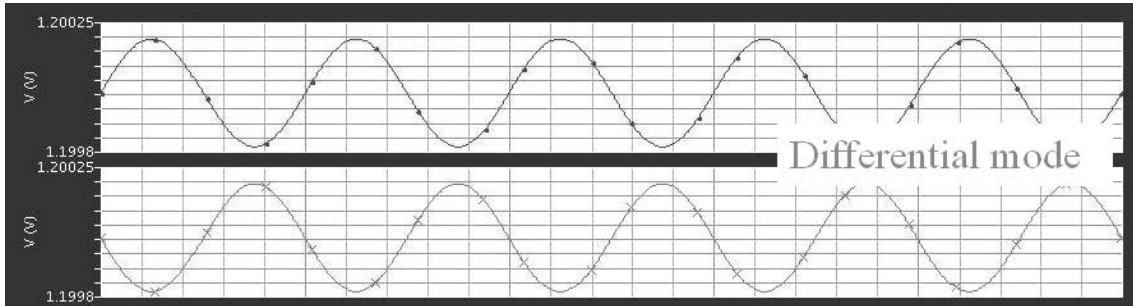


Fig. 3.5 The differential-mode signal of node  $V_{x1}$  and  $V_{x2}$

Next we have to check if the common-mode signals are successfully subtracted. We input two 0.1mV common-mode signals whose phases are the same and we can get the transient response shown in Fig.3.6, we can find that the common-mode signals are perfectly compressed to almost zero volt.

As a result, we have confirm that the method in (2.3) works. The noises (common-mode signals) have been canceled enormously. Next we will check the CMRR performance of the circuit.

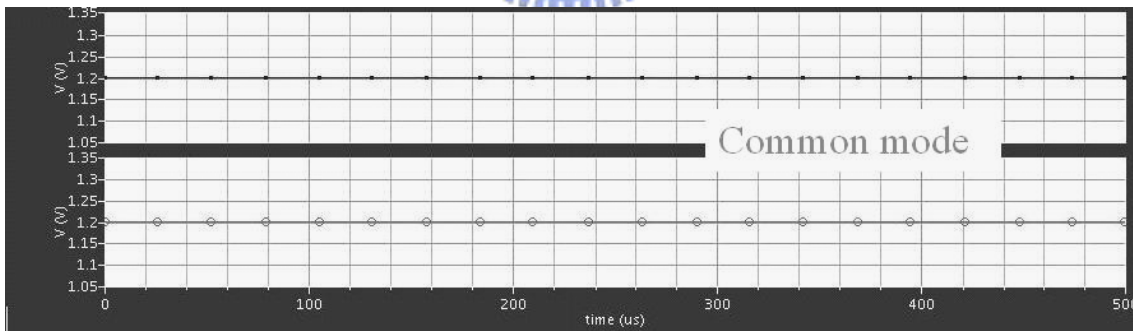


Fig. 3.6 The common-mode signal of node  $V_{x1}$  and  $V_{x2}$

Fig. 3.7 shows the frequency response of our new instrumentation amplifier. We can find that the CMRR can archive to the magnitude of 215 dB. It is a very high magnitude.

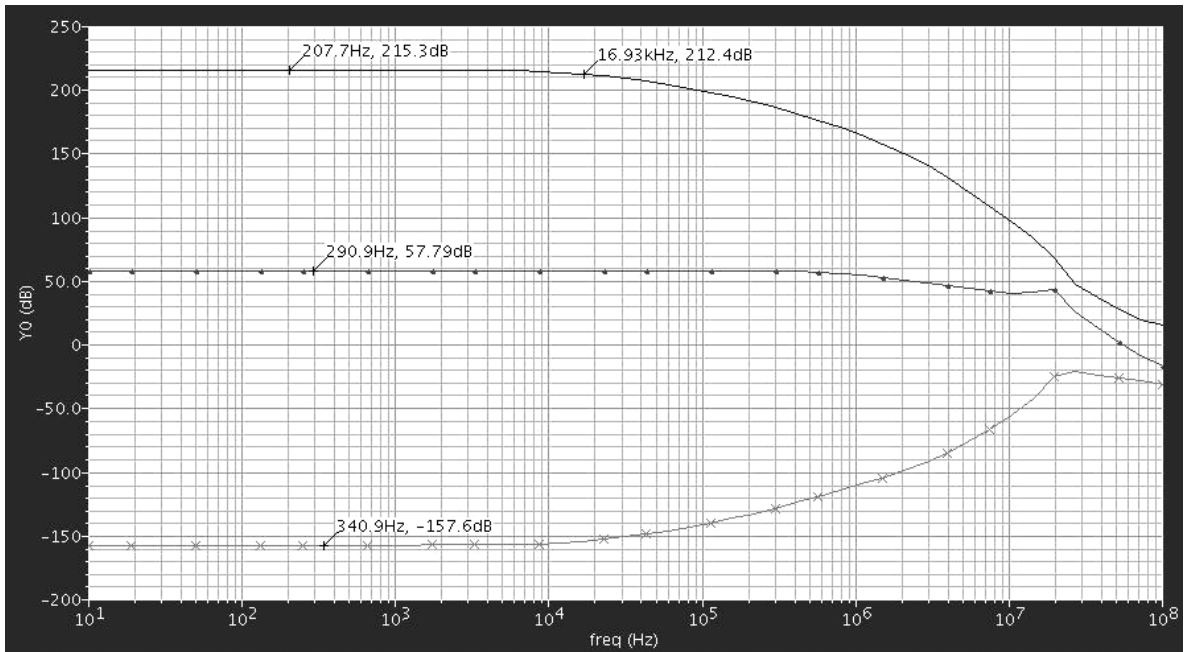


Fig. 3.7 The frequency response of the proposed INA structure

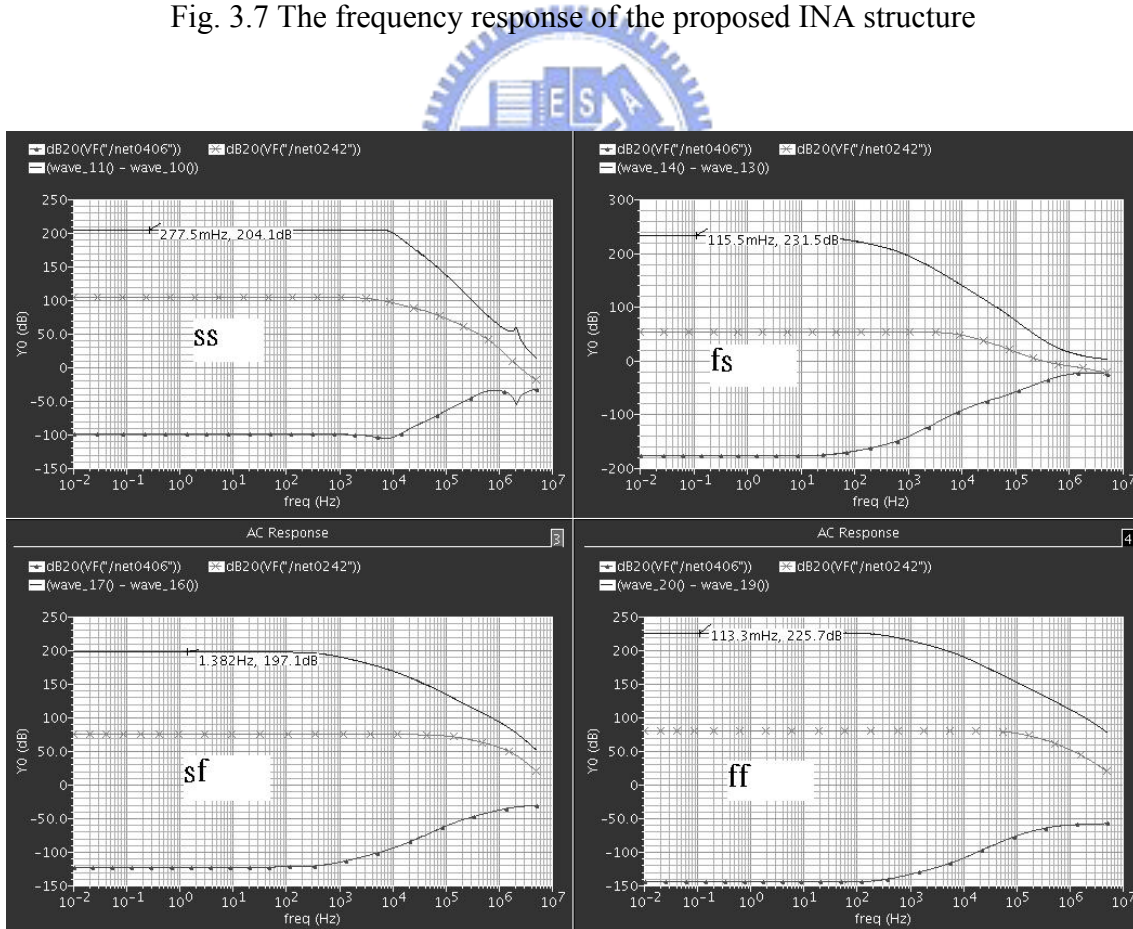


Fig. 3.8 The frequency response of the proposed INA structure with four corners

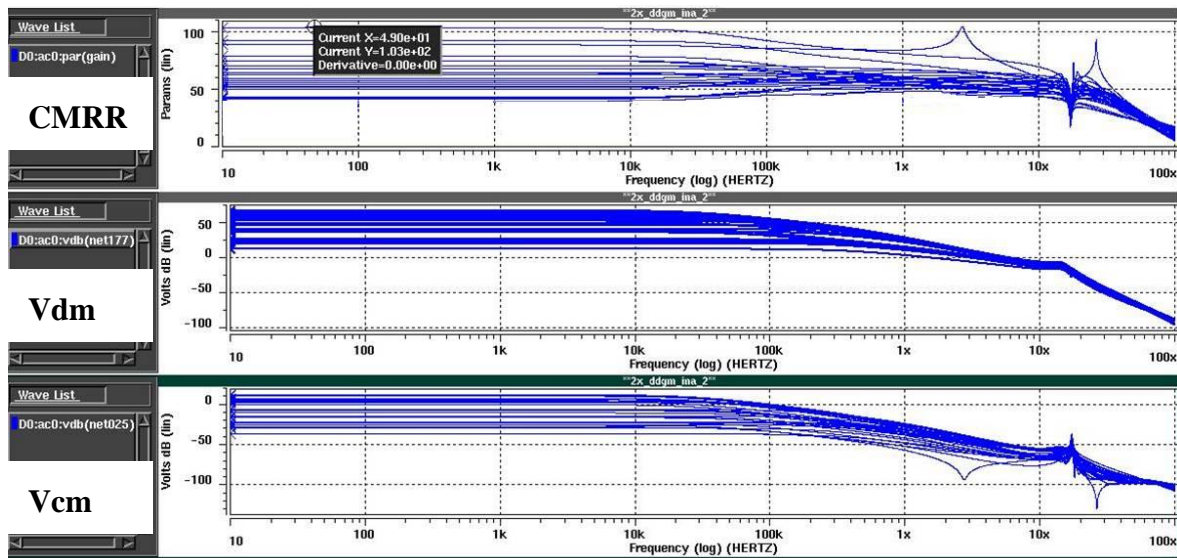


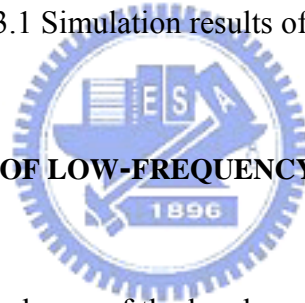
Fig. 3.9 The HSPICE Monte-Carlo simulation of the frequency response of the

proposed INA structure

Fig. 3.8 shows the simulation results of frequency response of INA with four corners and we can find that the CMRR range can still maintain from 197.1dB to 231.5dB. Fig. 3.9 is the Monte-Carlo simulation results of the frequency response of the proposed INA. We put 5% device mismatch in the HSPICE Monte-Carlo simulation and from Fig. 3.9 we can find that the CMRR degrades seriously from 40 to 103dB. This serious degradation is caused by the first stage of the subtraction function. Table 3.1 shows the simulation results of the proposed INA with the comparison of perfect and 5% device mismatch. We can find the most obvious different between the simulation result is the CMRR which degrades from 200~250dB to 40~100dB. As a result, we have to solve this problem in the future work.

Perfect Matching		Mismatch situation (5% device mismatch)	
Vdd	3.3V	Vdd	3.3V
Tuning gain	10~60dB	Tuning gain	10~60dB
CMRR	200~250dB	CMRR	40~103dB
$f_{3dB}$	2~16 kHz	$f_{3dB}$	2~16kHz
Output swing	+0.4V~-0.4V	Output swing	+0.38~ -0.35
Power	0.1mW	Power	0.1mW

Table 3.1 Simulation results of the INA



### 3.4 SIMULATION RESULTS OF LOW-FREQUENCY BANDPASS FILTER

We have simulated the ideal case of the bandpass LC ladder shown in Fig. 2.12(a) and filter with ideal Gm in Fig. 2.18.

Fig. 3.10 shows the simulation result of the bandpass Gm-C Elliptic filter with leapfrog structure using the Gm amplifier we design in chapter 2.3. Due to the tradeoff of the output resistance and the bandwidth of the Gm amplifier, we can't design a very high output resistance with high bandwidth we want. As a result, the simulation result have some different with the ideal case.

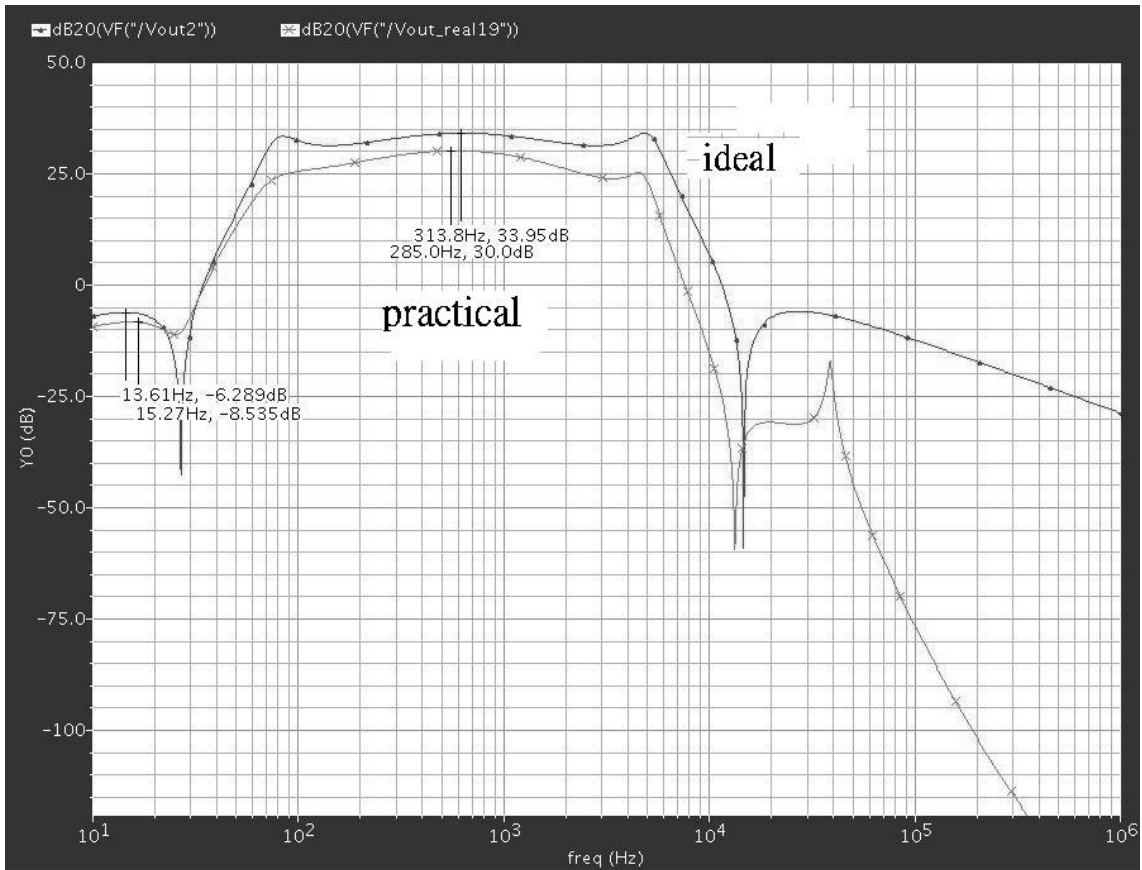


Fig. 3.10 Simulation results with the comparison of the ideal and the realistic filter

. From Fig. 3.10's comparison, we can find the attenuation decreases to 38.5 dB, and the passband ripple increase to 7dB. And we design a 30dB gain in the passband.

Fig. 3.11 shows the simulation results with four corners, we can find the frequency range of the filter drifts when  $f_s$  and  $f_f$ . However, we can use the tunable Gm amplifier to change the frequency range that drifts back to the frequency range we want.

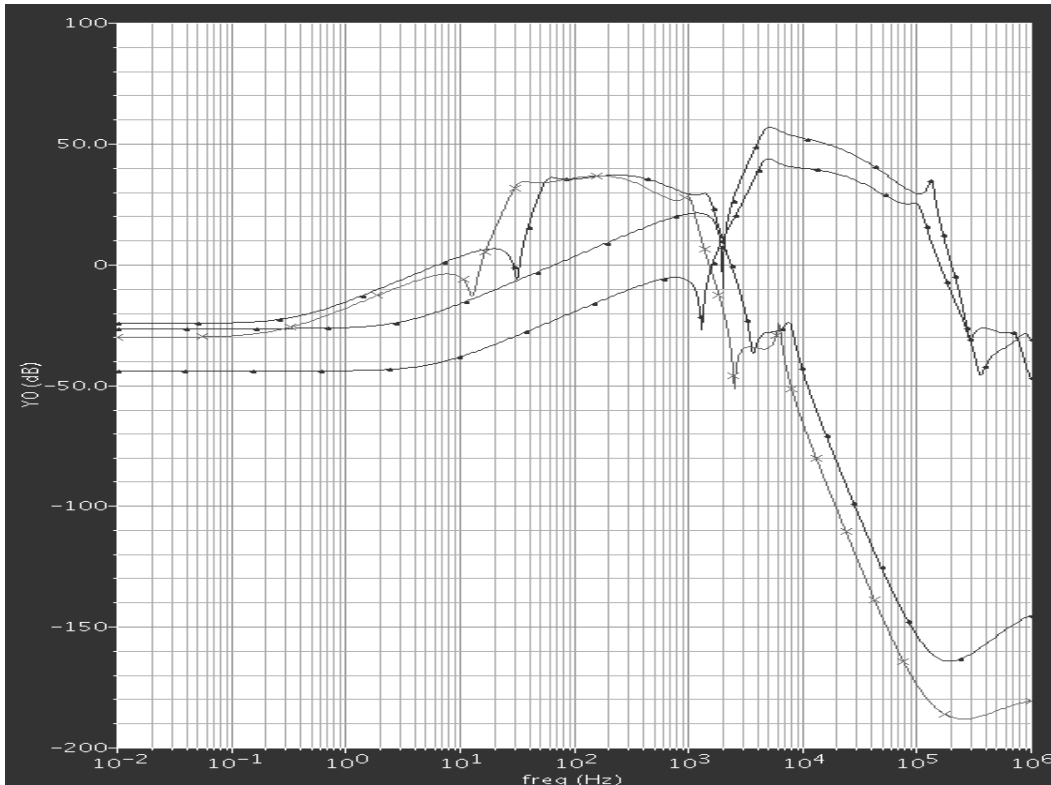


Fig. 3.11 Simulation results of the low-frequency BP filter with four corners

Filter	Spec	Simulation
Low corner frequency	50 Hz	50Hz
High corner frequency	2 kHz	2kHz
Stop band ratio	1.98	2.0
Stop band attenuation	40 dB	38.5dB
Pass Band Ripple	3 dB	7dB
Gain	>0dB	30dB
Power Dissipation	NA	130uW (39.28uA)
Type of the Filter	Elliptic	

Table 3.2 Simulation results of the low-frequency BP filter

### 3.5 WHOLE SIMULATION OF THE FRONT-END ELECTROPHYSIOLOGICAL SIGNAL MEASUREMENT SYSTEM

Fig. 3.12 shows the simulation result of the whole front-end of the electrophysiological measurement system which is composed of instrumentation amplifier and low-frequency bandpass filter. The upper curve is the differential mode and the lower one is the common-mode.

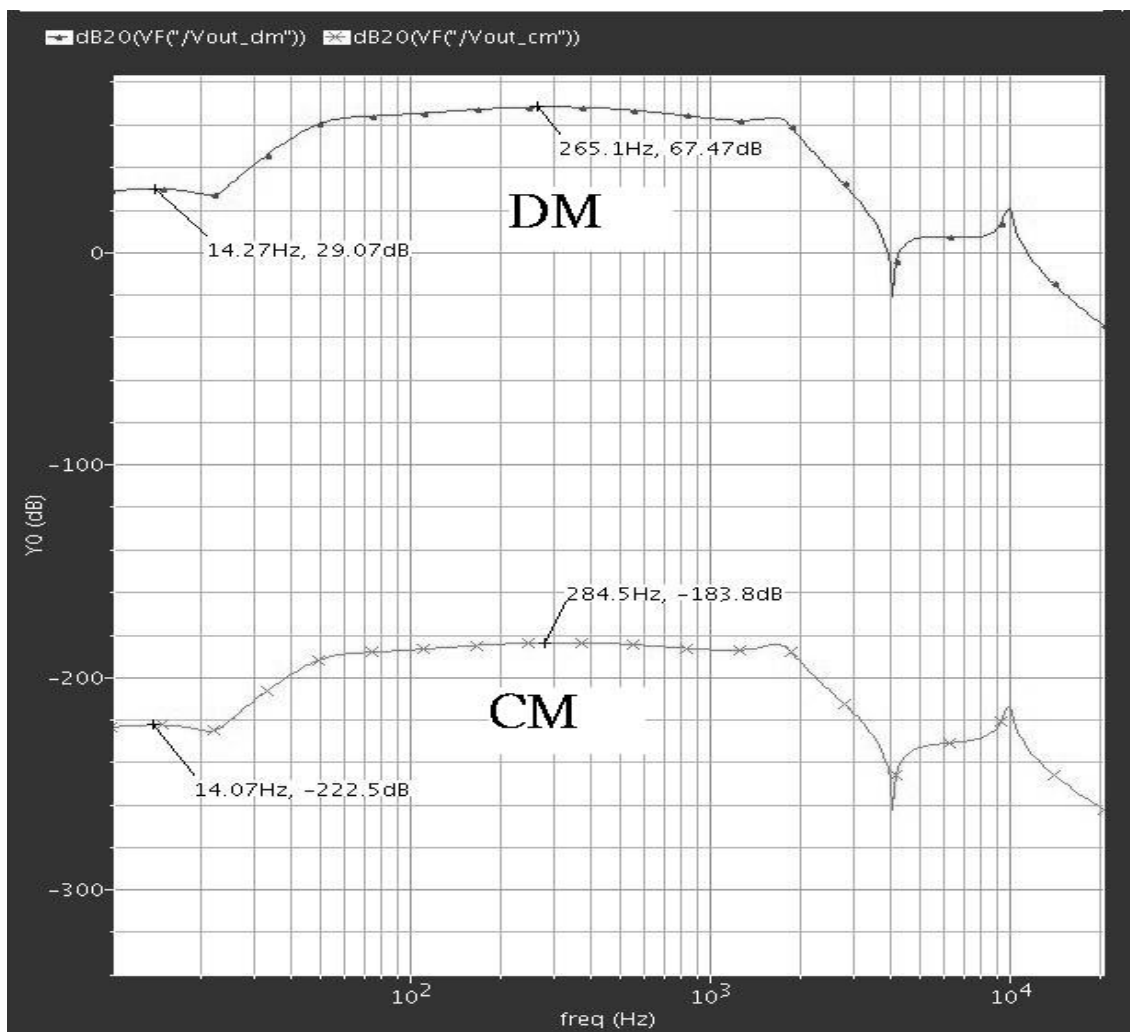


Fig. 3.12 The differential and common mode simulation results front-end circuit of the electrophysiological measurement system



Table 3.3 shows the simulation results of the front-end circuit of the electrophysiological signal measurement system. The CMRR can achieve 200~250dB and tunable gain from 10 to 120dB. The frequency range is from 50Hz to 2kHz. The total power consumption is 230uW.

<b>Simulation results of INA+Filter</b>	
CMRR	200-250dB
Voltage Gain	10-120dB
Frequency range	50Hz~2kHz
Stop band ratio	2.0
Stop band attenuation	38.5dB
Pass Band Ripple	7dB
Power dissipation	230uW

Table 3.3 Simulation results of the front-end circuit of the electrophysiological signal measurement system

## CHAPTER 4

### CONCLUSIONS AND FUTURE WORKS

---

#### 4.1 CONCLUSIONS

With combination with wireless network, home nursing and remote medical care will be indispensable in the future. In this thesis, we have designed the front-end circuit of the electrophysiological measurement system. We announced a new structure of instrumentation amplifier and designed a low-frequency bandpass filter using 5<sup>th</sup>-order Elliptic type and leapfrog structure.

For achieve high CMRR INA, we design a new analog block called differential difference operational transconductance amplifier (DDGm) with the similar operation principle as differential difference amplifier (DDA). Our new structure of INA proposed in the thesis is constructed with two differential difference Gm amplifiers and one Gm amplifier. The new INA can achieve high common-mode rejection ratio with tunable gain


After the INA, there is the bandpass filter with very low frequency between 50 Hz to 2 kHz. We use leapfrog structure to minimize the sensitivity of the filter to element value variations. The process of how to transfer a LC network to a leapfrog Gm-C filter is describe in detail. Due to the high Rs of the LC network that after normalized, we have to design the Gm amplifiers with small Gm value. So we have to use MOS in subthreshold region to obtain the small Gm value. Although small Gm value will encounter the problem of subthreshold current, we propose a method to solve it in this thesis. For the tunable Gm amplifier, we use a flipped voltage follower (FVF) to solve the problem of voltage follower which change its gain by output loads in most of the

tunable Gm amplifier.

For very low frequency filters, there are some critical design issues. We need very high output resistance to reduce the equivalent parasitic resistance. However, the corner frequency of the Gm amplifier is inverse proportional to output resistance. As a result, the bandwidth and the output resistance is a tradeoff design parameter. So we have to do the MOS size optimum to achieve the best performance of the Gm amplifier.

For the whole front-end circuit of the electrophysiological signal measurement system, we designed with TSMC 0.35um technology and the whole chip has a 230 micro-watt power consumption. With the very small power dissipation and high CMRR value with insensitive filter, we've successful designed a high performance front-end circuit of the electrophysiological signal measurement system.

## 4.2 FUTURE WORKS



Although we have proposed a instrumentation amplifier with high CMRR, the CMRR value is still affected by the process variation. The CMRR degrades when we run Monte-Carlo simulation, and we have to think some solution to solve it. It can also called the input offset problem. Many papers [15] announced the method of chopper amplifier to eliminate input offset problem. It maybe a good idea to combine our INA with switches to solve the problem. Another problem of the INA is the input referred noise that would also be a problem of the INA. We have to model the noise and find the way to optimize the input referred noise.

For very low-frequency using leapfrog structure, we will encounter the problems we have discussed in the chapter2. The tradeoff between output resistance and the bandwidth of the Gm amplifier need to be solved by new Gm amplifier circuit. If the tradeoff is limited by technology, we can also use 0.18um technology to simulate the

filter and we will have much more margin to design the Gm amplifier.

For the front-end circuit of the electrophysiological signal measurement system, low power and high CMRR is the most critical part of it. We have designed a low power and high CMRR circuit. In the our future work, we will also integrate the analog to digital converter (ADC), wireless part, and digital process circuits to a single chip. Once the single chip is realized, it will be a memorable achievement of the combination of IC technology and medical. Also our live will be changed when that day comes. The layout, fabrication, and measurement of the front-end circuits of the electrophysiological signal measurement system will go through after the simulation.



## REFERENCES

- [1] The home hospital, IST (Information Society Technologies) 2001, Technologies Serving People, European Commission, Edited by MS Consulting Birmingham, pp. 22-23.
- [2] A. A. Al-Imari, K. A. Rashid, and M. Al-Dagstany, "Telemetry based system for measurement and monitoring of biomedical signals," Proceedings of The 3<sup>rd</sup> *IEEE International Workshop on System-on-Chip for Real-Time Applications*, 2003, pp. 352-356.
- [3] Wen-Yaw Chug\*, Kang-Ping Lin, Chih-Jen Yen, Cheng-Lun Tsai, and Te-Shin Chen "Analog Processor Chip Design for the Bio-signal Readout Circuit Application" *BMES/EMBS Conference, 1999. Proceedings of the First Joint*, Volume 2, 13-16 Oct. 1999 Page(s):881 vol.2
- [4] C. Toumazou, F.J. Lidgey and C.A. Makris "Extending voltage-mode op amps to current-mode performance" *IEE Proceedings*, Vol. 137, Pt. G, No. 2, April 1990
- [5] A. Sedra and K. C. Smith, "A Second-Generation Current Conveyor and Its Applications" *IEEE Transactions Circuit Theory*, February 1970
- [6] Kimmo Koli and Kari A. I. Halonen, "CMRR Enhancement Techniques for Current-Mode Instrumentation Amplifiers", *IEEE Trans. on CAS*, Vol. 47, No. 5, May 2000
- [7] Seyed Javad Azhari and Hossien Fazlalipoor, "A Novel Current Mode Instrumentation Amplifier (CMIA) Topology" *IEEE Transactions on Instrumentation AND Measurement*, Vol. 49, No. 6, December 2000
- [8] E.L.Douglas, D.F. Lovely, and D.M. Luke "A Low-voltage Current-Mode Instrumentation Amplifier Designed in a 0.18-Micron CMOS Technology" *CCECE 2004-CCGEI*, Niagara Falls, May 2004
- [9] E. Abou-Allam and E.I. El-Masry, "High CMRR CMOS current operational amplifier" *Electronics Letters*, 23rd June 1994 Vol. 30 No. 73
- [10] Pietro Andreani, and Sven Mattisson, "On the Use of Nauta's Transconductor in Low-Frequency CMOS gm C Bandpass Filters" *IEEE Journal Of Solid-State Circuits*, Vol. 37, No. 2, February 2000
- [11] B. Nauta, "A CMOS transconductance-C filter technique for very high frequencies," *IEEE J. Solid-State Circuits*, vol. 27, pp. 142-153, Feb.1992.

- [12] Lin, C.-H.; Pimenta, T.; Ismail, M. "A low-voltage low-power CMOS V-I converter with rail-to-rail differential input for filtering applications" *Electronics, Circuits and Systems*, 1998 IEEE International Conference on Volume 1, 7-10 Sept. 1998 Page(s):165 - 168 vol.1
- [13] J. F. Duque-Canillo, G. Torelli, R. P. Crez-Aloe, J. M. Valverde, and F. Maloberti "Fully Differential Basic Building Blocks Based on Fully Differential Difference Amplifiers with Unity-Gain Difference Feedback" *IEEE Transactions On Circuit And Systems-I: Fundamental Theory And Applications*, Vol. 42, No. 3, March 1995
- [14] Carvajal, R.G.; Ramirez-Angulo, J.; Lopez-Martin, A.J.; Torralba, A.; Galan, J.A.G.; Carlosena, A.; Chavero, F.M., "The flipped voltage follower: a useful cell for low-voltage low-power circuit design" *IEEE Transactions On Circuits And Systems-I: Volume 52, Issue 7, July 2005* Page(s):1276 - 1291
- [15] Soliman A. Mahmoud and Ahmed M. Soliman "The Differential Difference Operational Floating Amplifier: A New Block for Analog Signal Processing in MOS Technology" *IEEE Transactions On Circuit And Systems—II: Analog And Digital Signal Processing*, Vol. 45, No. 1, January 1998
- [16] Qiuting Huang and Christian Menolli "A 200nV Offset 6.5nV/JHz Noise PSD 5.6kHz Chopper Instrumentation Amplifier in Igm Oigital CMOS" *IEEE international Solid-State Circuits Conference 2001*
- [17] Christian Hristian C. Enz, Eric A. Vittoz and Fran~Ois Krummenacher "A CMOS Chopper Amplifier" *IEEE Journal Of Solid-State Circuits*, Vol. Sc-22, No. 3, June 1987
- [18] Anton Bakker, Kevin Thiele', and Johan Iiuijsing "A CMOS Nested Chopper Instrumentation Amplifier with 100nV Offset" *IEEE International Solid-state Circuits Conference 2000*
- [19] Paul D. Walker, and Michael M. Green, "An Approach to Fully Differential Circuit Design without Common-Mode Feedback" *IEEE Transactions On Circuits And Systems-II: Analog And Digital Signal Processing*, Vol. 43, No. 11, November 1996
- [20] Sukhum Luikitmongkol, Wandee Petchmaneelumka, Vanchai Riemja, Chaleompun Wangwiwattana, and Amphawan Chaikla "A Low-voltage CMOS Instrumentation Amplifier" *SICE 2003 Annual Conference Volume 3*, 4-6 Aug. 2003 Page(s):2995 - 2998 Vol.3
- [21] Jordi Sacrist'an, Ma Teresa Os'es 'Low Noise Amplifier For Recording ENG Signals In Implantable System" *Circuits and Systems, 2004. ISCAS '04. Proceedings of the 2004 International Symposium on Volume 4*, 23-26 May 2004 Page(s):IV - 33-6 Vol.4

- [22] Michel S. J. Steyaert, Willy M. C. Sansen, and Chang Zhongyuan “A Micropower Low-Noise Monolithic Instrumentation Amplifier For Medical Purposes” *IEEE IEEE Journal Of Solid-State Circuits*, Vol. Sc-22, No. 6, December1987
- [23] C. Toumazou, F.J. Lidgey and C.A. Makris “Extending voltage-mode op amps to current-mode performance” *IEE Proceedings*, Vol. 137, Pt. G, No. 2, April 1990



## VITA

姓名：林韋霆

性別：男

出生日期：民國69年4月19日

出生地：台灣省台北市

住址：台北市慶城街23-7號5F

學歷：

國立清華大學工程與系統科學系畢業 (87年9月-91年6月)

國立交通大學電子研究所碩士班 (91年9月-95年6月)



論文名稱：新型低功率與高雜訊抑制電生理訊號量測系統之  
前端電路設計與分析

**THE DESIGN AND ANALYSIS OF NEW LOW POWER  
HIGH CMRR CMOS FRONT-END CIRCUITS FOR  
ELECTROPHYSIOLOGICAL SIGNAL MEASUREMENT  
SYSTEM**